

## Report

Project No. 33486

# Neutron Absorber Material Corrosion Testing Final Report FY2021

Tedd E. Lister  
Ronald E. Mizia  
Luis A. Diaz  
Henry C. Hutcheson  
Abenchara M. Betancor Abreu




The INL is a U.S. Department of Energy National Laboratory  
operated by Battelle Energy Alliance.

**Idaho National Laboratory**

**Neutron Absorber Material Corrosion  
Testing Report**

Identifier:	
Revision:	0
Effective Date:	09/17/2021
	Page: 1 of 51

**Prepared by:**

  
\_\_\_\_\_  
Tedd E. Lister

09/17/2021  
\_\_\_\_\_  
Date

**Approved by:**

  
\_\_\_\_\_  
Joshua Jarrell

09/17/2021  
\_\_\_\_\_  
Date



<b>Neutron Absorber Material Corrosion Testing Report</b>	Identifier: Revision: 0 Effective Date: 09/17/2021
---	--

Page 3 of 51

## Acronyms

AAS –	atomic absorption spectroscopy
ASTM –	ASTM International
ANA –	Advanced Neutron Absorbing Alloy
BB –	Bohler Bleche
BSS –	borated stainless steel
CarTech –	Carpenter Technology Corporation
COTS –	commercial of the shelf
CPP –	cyclic potential polarization
DOE –	Department of Energy
$E_{\text{corr}}$ –	corrosion potential
EDS –	energy dispersive spectroscopy
$E_{\text{pit}}$ –	pitting potential
$E_{\text{rp}}$ –	repassivation potential
ICP-MS –	inductively coupled plasma – mass spectrometry
INL –	Idaho National Laboratory
LLNL –	Lawrence Livermore National Laboratory
LPR –	linear polarization resistance
NAM –	neutron absorbing material
NSNFP –	National Spent Nuclear Fuel Program
NRC –	Nuclear Regulatory Commission
ORNL –	Oak Ridge National Laboratory
OCRWM –	Office of Civilian Radioactive Waste Management
PREN –	pitting resistance equivalent number
RO –	reverse osmosis
SNF –	spent nuclear fuel
SNL –	Sandia National Laboratory
SAM –	structurally amorphous materials

**Idaho National Laboratory****Neutron Absorber Material Corrosion  
Testing Report**

Identifier:

Revision: 0

Effective Date: 09/17/2021

Page 4 of 51

SS – stainless steel  
WPOB – waste package outer barrier  
XRD – x-ray diffraction

**Idaho National Laboratory****Neutron Absorber Material Corrosion  
Testing Report**

Identifier:

Revision: 0

Effective Date: 09/17/2021

Page 5 of 51

**1. Introduction**

Neutron absorbing materials (NAMs) are used within commercial spent nuclear fuel (SNF) canisters to maintain nuclear subcriticality in storage. Including NAMs within commercial SNF canisters absorbs neutrons and thereby reduces the potential for criticality events. For the FY2020, Idaho National Laboratory (INL) was tasked with reviving the corrosion testing portion of a neutron absorber development program supported by the National Spent Nuclear Fuel Program (NSNFP) and later by the Office of Civilian Radioactive Waste Management (OCRWM). Previous work focused on two classes of materials: commercially produced borated stainless steels (BSSs) and INL-developed nickel-based alloys with gadolinium added as a neutron absorber. This report will provide results from corrosion testing performed during FY2021. The testing was performed according to INL PLN-6266, which was formulated through consensus with staff at Oak Ridge National Laboratory (ORNL), Sandia National Laboratory (SNL), and INL [1].

**1.1 Testing approach**

Corrosion evaluations are inherently difficult, presenting many challenges and limitations. When possible, examination using in-service conditions is the best approach. However, in the problem being faced pertaining to long-term SNF storage, neither the service conditions nor the vast service time required can be replicated. This has posed a challenge in predicting the long-term behavior of materials used in repositories. The approach used in assessing NAMs leverages the electrochemical testing scheme previously employed in developing a comprehensive corrosion model [2].

Corrosion can be categorized into two broad types: general (uniform) corrosion and localized corrosion. The approach taken in this work is to examine both types. General corrosion is a relatively uniform process in which the metal is reduced in thickness. This can be ascribed a linear rate, such as millimeters per year (mmpy). For engineered structures, the environmental conditions across all surfaces vary and thus may not appear uniform when viewed macroscopically. Localized corrosion is much more challenging and potentially damaging compared to general corrosion. Localized corrosion is a general term for several types (mechanisms) of corrosion that attack at specific places on surfaces. Such attacks can be driven by microstructural and physical aspects of the engineered structure, as well as by the localized environment. Alloys tend to have non-uniform compositions (such as secondary phases, welds, and grain boundaries) that may result in areas with greater susceptibility to localized corrosion. Environmental factors such as crevices (where surfaces are held against other surfaces) can limit the free diffusion of chemicals from the surface and result in corrosive conditions. Galvanic effects are also

<b>Neutron Absorber Material Corrosion Testing Report</b>	Identifier:
	Revision: 0
	Effective Date: 09/17/2021

Page 6 of 51

possible, with dissimilar metals in ohmic contact interacting such that one of the metals acts as the corroding anode.

Pitting corrosion, the most common form of localized corrosion, is often described as having an initiation event followed by a growth phase [3]. The initiation event is the birth of a pit, which may or may not transition to growth and may involve significant latency. The growth phase occurs as the initiated pit continues to oxidize metal at the site. The growth may continue or repassivate, with oxide reforming over the metal.

The testing protocol employed in this work was based on those used previously to model waste package outer barrier (WPOB) corrosion [2]. An electrochemical test sequence based on these evaluations was used to evaluate both localized and general corrosion [4]. General corrosion was assessed using linear polarization resistance (LPR). The magnitude of the current (slope) near  $E_{\text{corr}}$  is proportional to the general corrosion rate [5]. A more challenging assessment is that for localized corrosion. Electrochemical tests were used to determine three important potentials: (1)  $E_{\text{corr}}$ , (2) pitting potential ( $E_{\text{pit}}$ ), and (3) repassivation potential ( $E_{\text{rp}}$ ). These parameters are described in more detail in Section 1.2 below. The localized corrosion model for the WPOB employed electrochemical testing to determine these parameters. For evaluation purposes, numerical models were built for both  $E_{\text{corr}}$  and  $E_{\text{rp}}$ , based on varying ion composition and temperature [2]. This work will not develop a comprehensive environmental model, as it is more of a comparative materials evaluation using three solutions at one temperature, with seawater considered the most relevant condition.

## 1.2 Testing methods

$E_{\text{corr}}$  is a mixed potential in that it is set by a balance of anode and cathode reactions occurring on the specimen surface. For most service conditions, corrosion is not driven externally (except by galvanic corrosion driven by the differential potential of two metals); thus, by definition, it occurs at  $E_{\text{corr}}$ . The cathode reaction is either  $\text{O}_2$  reduction or  $\text{H}_2$  production, depending on the specimen and environment. In general, as the anode corrosion increases, the observed potential shifts negative as the cathode reaction increases. A transient behavior is observed when the driving force for corrosion is at the edge of stability, resulting in alternating corrosion-passivation events. In the case of localized corrosion, this could be driven by a single pit or behavior distributed across the surface.

Cyclic potential polarization (CPP) tests were performed following the LPR tests. The CPP tests provide an understanding of the specimen's corrosion and electrochemical characteristics in the tested environment as a function of potential. Figure 1 shows a diagram of a CPP curve for a metal that is susceptible to pitting corrosion. For most metals and alloys, the electrochemical response can be broken

## Idaho National Laboratory

<b>Neutron Absorber Material Corrosion Testing Report</b>	Identifier: Revision: 0 Effective Date: 09/17/2021
---	--

Identifier: Revision: 0 Effective Date: 09/17/2021	Page 7 of 51
--	--------------

down into three regions: the active region, the passive region, and the pitting region. The current is plotted as an absolute value in log scale. The active region is centered around  $E_{\text{corr}}$ , which is defined by a complex balance of chemical reactions that sets the potential relative to a reference electrode. It is the point where currents for these reactions are balanced—such that, when the potential is manipulated (using a potentiostat and electrochemical cell), the net current increases in either direction. The scan is initiated negative of the measured  $E_{\text{corr}}$  in the positive direction. After passing through  $E_{\text{corr}}$  (note that, in this study, we report  $E_{\text{corr}}$  with air purge and not based on the CPP curve), the net current flips from cathodic to anodic, and, depending on the environment, a broad hump may be observed which is the anodic dissolution of the metal in what is called the “active” region. This peak often decreases as the oxide layer reforms in the passive region, the oxide layer being stabilized by the more positive potential. In relatively benign environments (for the metal/alloy), the current in the active region may be very small, without a defined peak. The current will eventually increase in the passive region, either due to pitting corrosion or, in some cases, transpassive corrosion (often more positive in non-pitting alloy/environment conditions). The initiation of pitting corrosion is often preceded by noise spikes in current, due to pit initiation and repassivation before stable pitting sets in. Deeper into the pitting region, the current increases, and the sweep is reversed at the switching potential. If pitting has initiated on the specimen, the current will remain high on the return sweep until the potential is insufficient to sustain the pitting.  $E_{\text{rp}}$  is a potential assigned to describe when pits have repassivated on the return sweep. Going back to the switching potential, if the current decreases quickly and closely tracks the forward sweep, it is likely the specimen is not susceptible to localized corrosion under the tested conditions. In that case, the current observed is either oxide film growth or transpassive corrosion. The remainder of the sweep may show features similar to the forward sweep. Once the potential reaches the starting potential, the test is stopped.



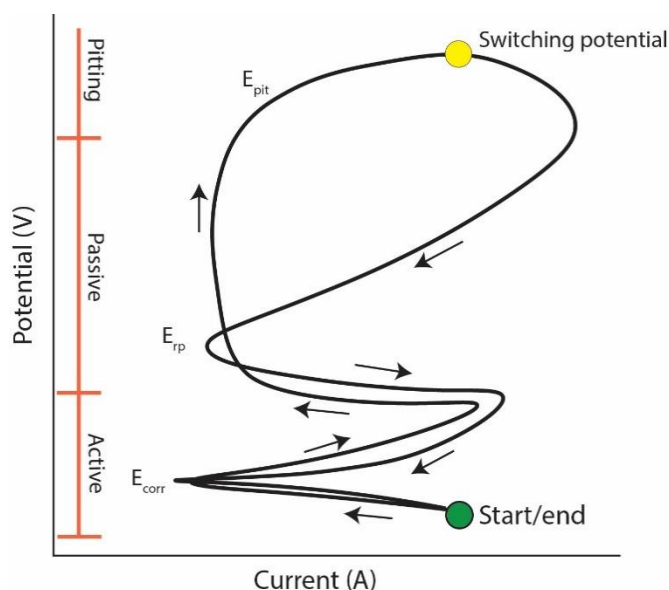


**Figure 1.** Diagram of a generic CPP curve.

Two important parameters are obtained from the CPP curves: the pitting potential ( $E_{pit}$ ) and  $E_{rp}$ .  $E_{pit}$  is defined as the point at which a sharp increase in current is observed in the forward sweep, where pitting is initiated.  $E_{rp}$  is defined as the point at which the current from pitting has subsided—typically the point at which the current switches sign (net current is negative) or crosses the forward sweep. This would indicate the point at which the material is defined as being stable (to pitting corrosion). Stability is assessed by comparing measured  $E_{rp}$  to  $E_{corr}$ , where the more positive  $E_{rp}$  is relative to  $E_{corr}$ , the less likely pitting corrosion will occur. Conversely, if  $E_{corr}$  is similar to or more positive than  $E_{rp}$ , the alloy and environment are considered incompatible, as localized corrosion is likely to occur. This was the basis for evaluating Alloy 22 as a WPOB material, with a parameterized model formulated and used to predict crevice corrosion [2].

Potentiostatic (PS) tests were performed to evaluate corrosion at specific potentials over time. The potential is selected based on values that are either near or somewhat positive of the  $E_{corr}$  value. If positive of the  $E_{corr}$  value, the tests provide a bounding case for corrosion or allow alloys to be compared under aggressive or accelerated conditions. The electrochemical cell and specimen geometry is the same as used for CPP tests. Figure 2 shows a diagram of a PS test for three different cases. The red curve is for a specimen that shows initiation but not sustained corrosion. Depending on the magnitude of current and duration, this could be minimal to significant corrosion but is where the specimen is on the edge of stability. This could be the case for stainless steel below the  $E_{pit}$  (see Figure 1) and positive of the  $E_{rp}$ . The blue line is an example of a specimen that has a short period of stability before corrosion initiates, but

then increases to significant and sustained corrosion, clearly unstable under the selected conditions. As pitting is a probabilistic, PS tests provide a longer time for pitting to initiate than in CPP tests. The green curve is a unique case which was observed for ANA specimens in previous work, where the secondary phase is preferentially dissolved, but corrosion slowly decreases as the secondary phase available to react at the surface decreases. The magnitude of current at the end of the test provides an indication for tendency to repassivate (reform protective oxide) following the secondary phase dissolution.

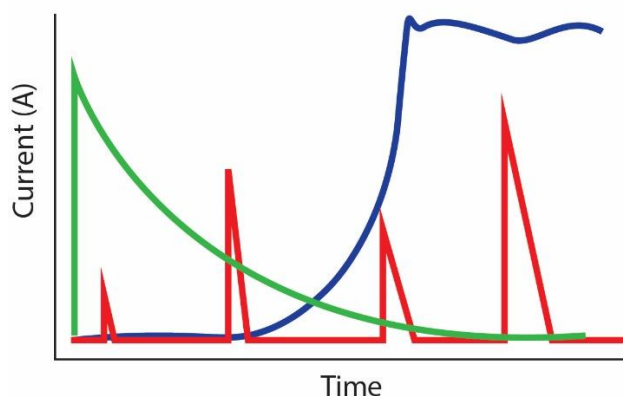


**Figure 2.** Diagram of PS tests for three different cases (see text).

While the approach to evaluating corrosion bears similarities to previous corrosion evaluations for waste package outer barriers, NAMs are not for containment; there is a lower functional requirement. The NAMs are likely to experience some localized damage if they remain largely intact and functioning to reduce criticality. Note that, as the material is likely to be exposed on both sides, the impact is doubled and must be factored into the design. This work is a materials selection activity that examines a small number of conditions for several different alloy types. Benchmark (non-NAM) alloys are included for comparison to leverage existing knowledge of their corrosion properties.

### 1.3 Testing environments

Aqueous corrosion is highly influenced by ion species and concentration. Chloride ions are known to promote localized corrosion of many forms, including pitting. A significant body of work centers around the stability of metals in chloride environments, particularly seawater. While chloride is known to promote corrosion, other ions such as nitrate and sulfate act as inhibitors of pitting corrosion. The basis condition for this work is seawater, a universal concentrated water [6]. Table 1 shows the top three anion components for seawater, indicating that chloride dominates the composition, followed by sulfate and

## Idaho National Laboratory

<b>Neutron Absorber Material Corrosion Testing Report</b>	Identifier:
	Revision: 0
	Effective Date: 09/17/2021

Identifier: Revision: 0 Effective Date: 09/17/2021	Page 10 of 51
--	---------------

carbonate. The ionic composition of seawater is much higher than that used previously for NAM testing, in which the total ionic content was 0.0045–0.0075 M [7].

**Table 1.** Anion composition of seawater [8].

Ion	Con (g/Kg)	Con (mol/kg)
chloride	19.353	0.54588
sulfate	2.701	0.0281
carbonate	0.142	0.00233

Testing was performed at 30°C using non-creviced specimens for initial evaluation and to provide data for making decisions as to what materials to select for further evaluation. Two other solutions were also used in this program: 0.028 M NaCl and 0.1 M HCl. The former was derived from a chloride solution used in testing funded by the National Regulatory Commission (NRC) and the Department of Energy (DOE) for assessing Alloy 22 [9-10]. The HCl solution can be viewed as a low-pH environment such as could be generated at a crevice. Both 0.028 M NaCl and 0.1 M HCl were used in INL testing of NAM materials [11].

## 2. Experimental

Testing was performed using ASTM G5 as a guide [12]. Experiments were performed according to step-by-step procedures, with checklists to ensure consistency. These checklists are companions to the laboratory notebooks that fully document the testing. The two testing stations are labeled to prevent identification issues. Tests were staggered to prevent specimens from being switched, as ID markings are not present on the specimens.

### 2.1 Specimens

#### 2.1.1 Wrought specimens

The following alloy types were tested: Type 304L stainless steel (SS), Type 316L SS, 304B4 SS, 304B5 SS, Alloy 22, M326 (low Cr) Advanced Neutron Absorber (ANA) and M327 (high Cr) ANA. The material compositions are shown in Table 2 below, as obtained from heat papers or through analyses performed in previous testing programs. Types 304L and 316L SS were obtained from Metal Samples Company, finished to 600 grit SiC. Alloy 22 specimens were also obtained from Metal Samples Company. ANA (also called Ni-Cr-Mo-Gd) specimens were remaining materials either machined by Metal Samples Company or the INL machine shop, finished to 600 grit SiC. BSS were those specimens remaining from previous testing activities.

## Idaho National Laboratory

Neutron Absorber Material Corrosion  
Testing Report

Identifier:

Revision: 0

Effective Date: 09/17/2021

Page 11 of 51

Table 2. Composition of alloys tested in this report.

Material	ANA	ANA	ANA	ANA	ANA	Alloy 22	304L	316L	C22Gd
Heat	M326	M327	M340	M322	D5- 8235	2277-7- 3130	D88180 A	AZ608	AMPC22 Gd1001
Nickel	Bal	Bal	Bal	Bal	Bal	Bal	8.41	10.5	Bal
Iron	0.025	0.032				3.54	Bal	Bal	3.1
Chromium	14.71	21.01	15.25	14.93	16.75	21.55	18.27	16.57	21.39
Molybdenum	14.53	14.32	14.07	14.71	14.43	13.47	0.33	2.018	13.04
Gadolinium	2	1.98	1.99	2.38	1.89				2.02
Oxygen	0.0032	0.0042							0.04
Nitrogen							0.069	0.034	0.03
Phosphorus						0.007	0.022	0.03	<0.01
Manganese	0.001	0.01				0.25	1.64		0.20
Magnesium	0.002	0.002							
Cobalt	0.009	0.003				0.74	0.12	0.21	<0.1
Carbon	0.006	0.001				0.003	0.02	0.022	0.012
Silicon	0.013	0.018				0.024	0.44	0.27	<0.01
Sulfur	0.001	0.002				0.004	0.024	0.0215	<0.01
Copper							0.35	0.31	<0.1
Vanadium						0.12			<0.01
Tungsten						2.83			2.93

The specimens were of the boldly exposed type (no intentionally designed crevices), with cylinders 1.7 in. in length and 0.25 in. in diameter attached to a threaded rod. The rod was isolated from contact with the solution by a glass tube with a flat Viton gasket sealing the submerged interface. For 304B4 and 304B5, crevice specimens were employed, as they were the only available specimens and material of that specification does not exist. The specimens were 0.75-in. x 0.75-in. x 0.375-in. blocks with a 0.325-in. through hole machined into the larger area surfaces. These specimens were tested without crevice assemblies. Teflon gaskets were used as seals between the glass and the specimen. The 304B5 specimens were refinished test specimens from previous work, as no untested specimens existed. Specimens were cleaned by being rinsed sequentially in acetone, ethanol, and deionized water to remove grease and other detritus prior to testing. The specimens were weighed on a 5-place balance both before and after testing. To assess ANA specimens in some tests, specimens were pickled in 1 M HCl in a small beaker at room temperature. Specimens tested in seawater were pickled for nine days, while the M327 tested in 0.1 M HCl was pickled for 29 days.

### 2.1.2 Cold-sprayed ANA specimens

**Idaho National Laboratory****Neutron Absorber Material Corrosion  
Testing Report**

Identifier:

Revision: 0

Effective Date: 09/17/2021

Page 12 of 51

Cold spray coating of the C22Gd specimens was performed at SNL and specimens shipped to INL. INL procured the AMP C22-Gd thermal spray powder from Haynes International with composition shown in Table 2. The ingot was powderized and a fraction with D50 of 25.21  $\mu\text{m}$  was isolated. Cold spraying was performed on 2" x 2" 316 stainless steel substrates were used for this study. Two sets of samples were used, one set which was grit blasted and the other which was left in the as-received state. Grit blasting was performed using alumina grit at 100 psig. Cleaning was performed on all samples using isopropyl alcohol to remove residual dirt, debris, or oils from machining or handling. The cold spray torch was rastered across the surface of the substrates in a square pattern. The pattern starts, stops, and turns around off the part to ensure uniformity in the coating. A step size of 1mm was used to improve uniformity by overlapping the deposition spot size by 90% of the previous traverse across the sample (spot size of the torch is ~10mm for most materials). A traverse speed of 400mm/s was used to achieve ~50-100 microns per pass of deposition. Coating was performed with a substrate temperatures of 600, 800, and 1100 °C. The 600 °C specimens were coated in He while the other two temperatures were coated in N<sub>2</sub>.

**2.2 Solution preparation**

Two test solutions are included in this work: artificial seawater (referred to simply as seawater) and 0.1 M HCl. The solutions were made using American Chemical Society (ACS)-grade chemicals. A calibrated three-place balance was used to weigh chemicals. These weights were recorded in laboratory notebooks and/or datasheets. Water was obtained via the reverse osmosis (RO) purification system, fed by a building RO water system. The final water conductivity was 18 M $\Omega$ -cm. The solution volume for the tests was 900 mL. ASTM D1141 was used as a guide for producing artificial seawater [8].

**2.3 Electrochemical cell**

The electrochemical cell was based on ASTM G5 specifications [12]. The cell and associated accessories were made of borosilicate glass. The cell has facilities for gas purging through a ceramic frit (150 cm<sup>3</sup>/min). A glass condenser, through which gas exited the cell, was employed to reduce water evaporation during the test. For ANA coated specimens and associated benchmark specimens, a commercial flat specimen cell was employed (Princeton Applied Research). Teflon gaskets were employed for sealing, where the exposed area was 0.83 cm<sup>2</sup>. Since the exposed area was significantly smaller than the specimen, up to four tests per specimen were performed under varying conditions. All electrochemical corrosion tests were performed at 30°C. The temperature was set through a thermocouple-controlled heating mantle. Thermocouples were checked for tolerance at INL calibration labs. A graphite rod was used as the counter electrode and was cleaned and/or replaced regularly. The flat specimen cell used a platinum mesh anode. Commercially sourced (Pine Instruments) reference

<b>Neutron Absorber Material Corrosion Testing Report</b>	Identifier:
	Revision: 0
	Effective Date: 09/17/2021

Page 13 of 51

electrodes of the Ag/AgCl (4 M KCl) type (0.199 V vs. normal hydrogen electrodes) were compared to two reference electrodes (of the same type and source) set aside specifically as standards.

#### 2.4 CPP Electrochemical testing sequence:

Electrochemical testing was performed using a prescribed sequence that (1) measures  $E_{\text{corr}}$  with air purge, (2) measures  $E_{\text{corr}}$  with  $N_2$  purge while removing the oxygen from Step 1, (3) performs three linear polarization resistance (LPR) tests, and (4) performs a CPP test from 0.2 V negative of the measured  $E_{\text{corr}}$  in  $N_2$ . LPR tests were performed by stepping from  $E_{\text{corr}}$  by -30 mV and sweeping positive 60 mV (a sweep of  $\pm 30$  mV of  $E_{\text{corr}}$ ). ASTM G59 was used as a basis for designing the tests [5]. For CPP, the anodic switching potential varied with specimen type, with SSs displaying excessive pitting if swept too far positive in comparison to nickel-based alloys. The scan rate for LPR and CPP testing was 0.6 V/hr (0.167 mV/sec).

#### 2.5 PS testing sequence:

PS tests were performed using an ASTM G5 type cell using boldly exposed specimens. Most of the specimens were of the cylindrical type (except M340 which was a crevice specimen tested without a crevice former attached). All potentiostatic tests were performed in simulated seawater. Test were primarily performed by holding the potential at 0.2 V vs Ag/AgCl for 50 hours. The test sequence was based on that used for the CPP tests, with the PS performed in place of the CPP test.

#### 2.6 Pickling of ANA specimens

ANA specimens were pickled in 1 M HCl for several days and periodically the solution was sampled. Flame atomic absorption spectroscopy (AAS) was used to identify Ni and Cr while inductively coupled plasma - mass spectrometry (ICP-MS) was utilized to determine concentrations of Gd. The molar ratio of Ni to Gd serves as a key tool in determining which phases in the alloy are dissolving.

#### 2.7 Post-test analysis

Data was analyzed using software included with the potentiostat. Specific calculations for corrosion rates were based on guidelines obtained from ASTM G102 [13]. The corrosion rate was calculated using EC-Lab software (Version 11.34) provided with the BioLogic potentiostat. For CPP curve analysis, the final  $E_{\text{corr}}$  in air provides a value for where the alloy potential resides in equilibrium with air. The pitting potential ( $E_{\text{pit}}$ ) was estimated as the potential where the current rapidly increases, and the  $E_{\text{rp}}$  was estimated as being the value at which the reverse sweep crossed zero current (switching from positive to negative). For SS specimens, this was not always observed, and the  $E_{\text{rp}}$  was chosen as the value at which a sharp deviation in the current drop on the return sweep occurred. Specimens were weighed both before and after testing, and the differences were reported. No attempt was made to descale specimens, and visually significant scaling was not observed.

<b>Neutron Absorber Material Corrosion Testing Report</b>	Identifier: Revision: 0 Effective Date: 09/17/2021
---	--

Page 14 of 51
---------------

## 2.8 Specimen and solution analysis

Several methods of post-test analysis have been employed: photography, optical microscopy, and scanning electron microscopy. Measurement of pit depths was also performed for some specimens, using an optical microscope with a z-calibrated motor. In the future, specimens will be available to perform other analysis methods, as deemed useful to interpret results. A volume of test solution was also captured and will be kept for possible future analysis, to be performed when deemed useful to interpret results.

## 3. Results

Results have been broken into sections for various testing activities.

### 3.1 Testing of Wrought ANA

The purpose of this activity was to assess dissolution of the active gadolinide ( $\text{Ni}_5\text{Gd}$ ) phase of the ANA material. As there is little Cr in this phase and Gd is a reactive metal (has a negative reduction potential), corrosion of the gadolinide phase is significant at low pH. The question which has not been fully answered in previous work is to what extent the ANA specimens repassivate after gadolinide phase dissolution. It has previously been speculated that after the surface exposed gadolinides were dissolved, that corrosion would cease. This was formulated based on what appeared to be a lack of connectivity between particles, suggesting the base material would effectively isolate particles deeper in the specimen. However, this was never fully examined and proven through longer term tests in somewhat aggressive conditions. It is known that the higher Cr containing M327 showed much lower current than other ANA specimens in potentiostatic (PS) tests [14]. These tests hold the specimen at a potential of choice, where 0.2 V was typically chosen as a slightly accelerated condition. In a comparison to Alloy 22, M327 showed current values which were similar and at times lower than Alloy 22 in dilute HCl [14].

#### 3.1.1 Acid pickling of ANA specimens

Acid pickling was performed as a method to remove the gadolinide secondary phase from the surface as a pretreatment before performing electrochemical corrosion tests. The results of these tests were presented in the FY2020 corrosion report [15] and additional evaluation is shown later in this report. The Ni/Gd molar ratio obtained from sampling acid pickling tests for M326 and M327 specimens is shown in Figure 3. A horizontal line is provided in the two graphs shows the ratio of Gd/Ni in the gadolinides (the Ni/Gd ratio of the bulk alloy is much higher, 92.0 in the case of M326 and 84.7 in M327) [14-15]. The Ni/Gd molar ratio in the pickling solution of M326 specimens starts near that of the secondary phase but trends upwards after two weeks reaching a ratio just below 8. This indicates that while the Gd-rich secondary phase accounts for most of corrosion, the Ni-based primary phase contributes as well. This is corroborated by the fact that significant amounts of Cr, higher than those explainable by trace amounts in

## Neutron Absorber Material Corrosion Testing Report

Identifier:

Revision: 0

Effective Date: 09/17/2021

Page 15 of 51

$\text{Ni}_5\text{Gd}$  (2.41% by weight [14-15]), were detected in the M326 pickling solution. This is shown in Figure 4, where the Cr concentration steadily increased with exposure time. For M326, the Ni and Gd continues to increase with exposure, however the Gd level appears to reach a plateau. This suggest further testing for longer periods would be required to assess if gadolinide dissolution was quenched. M326 exhibits some form of continuous corrosion, either the Gd rich secondary phase or some combination with the primary phase beyond 2 weeks. However, the rate of Gd dissolution appears to be tapering off near the end of this period. The highest extracted mass of Gd in any M326 pickling sample corresponds to 6.48% of the total Gd content, indicating  $\text{Ni}_5\text{Gd}$  corrosion is penetrating beyond that intersecting the specimen surface.

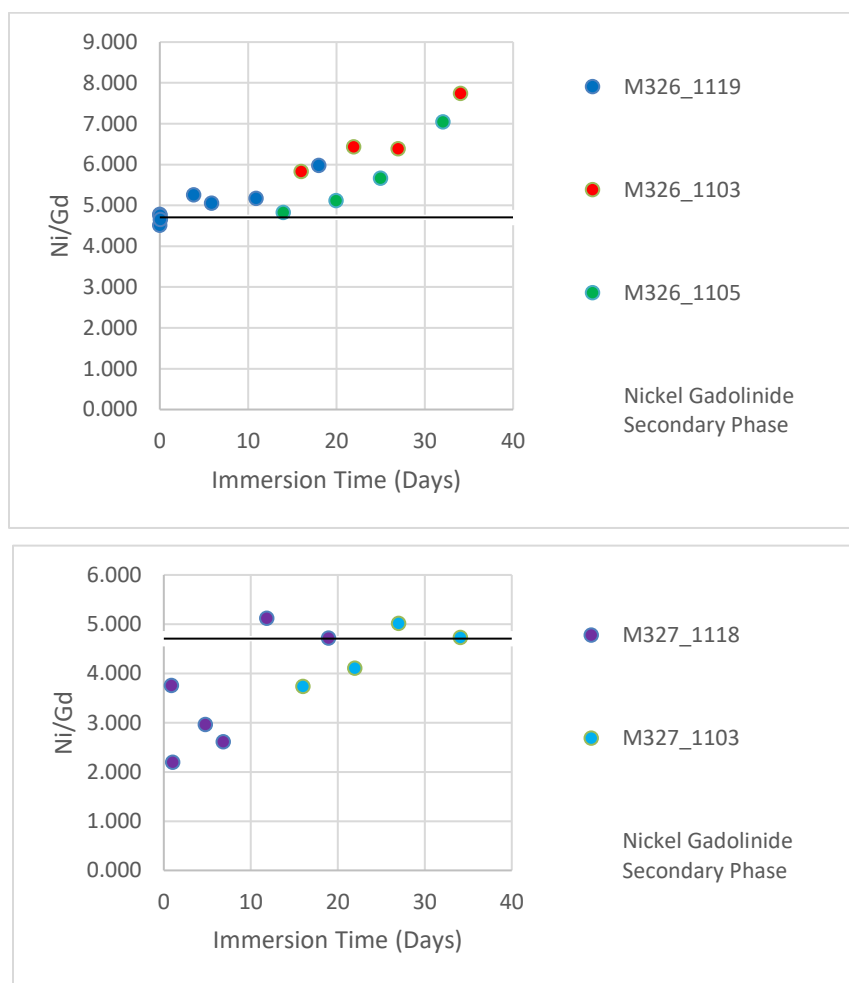


**Figure 3.** Evolution of Ni/Gd molar ratio in M326 (top) and M327 (bottom) acid pickling solution.



**Neutron Absorber Material Corrosion  
Testing Report**

Identifier:

Revision: 0

Effective Date: 09/17/2021

Page 16 of 51

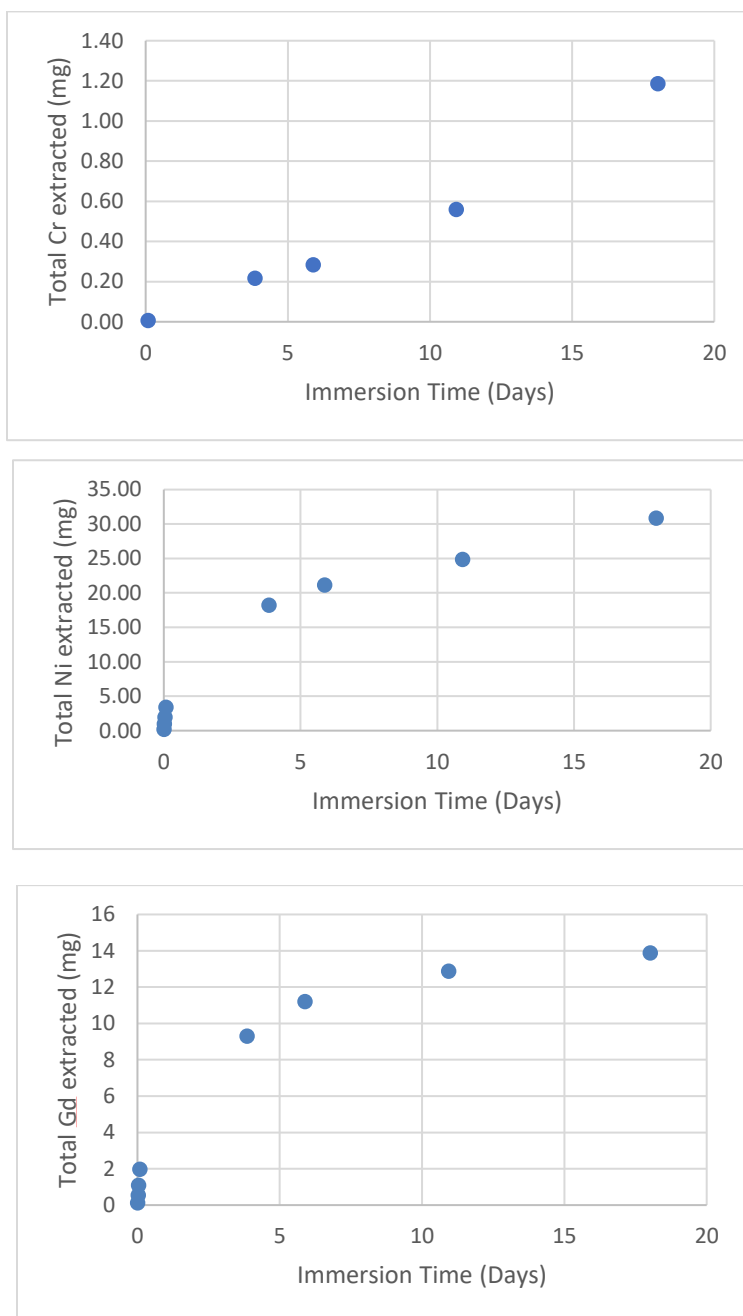


**Figure 4.** Total Cr, Ni and Gd extracted from M326 specimen during acid pickling.

In the case of M327 (Figure 3), the Ni/Gd molar ratio appears lower than that of the secondary phase for unknown reasons. After 12-20 days, the Ni/Gd molar ratio stabilizes around that which would be expected for dissolution of the gadolinide phase alone. This suggests that the gadolinides in the M327 material intersecting the surface dissolve but does not proceed further. Figure 5 shows the Ni and Gd content versus pickling time. Note that the level of Ni and Gd are over an order of magnitude lower. Cr

## Neutron Absorber Material Corrosion Testing Report

Identifier:

Revision: 0

Effective Date: 09/17/2021

Page 17 of 51

was not observed in the M327 acid pickling solution above the detection limit, further indicating that the primary phase remained stable in such a harsh environment. The results point to primarily Ni<sub>5</sub>Gd dissolution, which is not only significantly reduced in magnitude compared to M326, but also more definitively slow after 10 days. This is likely due to the higher Cr content in M327 stabilizing the primary phase. This could also be a microstructural effect involving the degree of interconnection for the gadolinides that needs further examination. The highest extracted mass of Gd in any M327 pickling sample corresponds to 0.23% of the total Gd content, indicating Gd loss was limited compared to that of M326. A calculation was made using the measured Gd in solution for each alloy and the specimen dimensions. The M326 which lost 6.2% of Gd weight indicated an impact depth of 78 μm, while M327 with 0.23% of Gd was impacted to a depth of 2.8 μm. This calculation assumes a uniform impact.

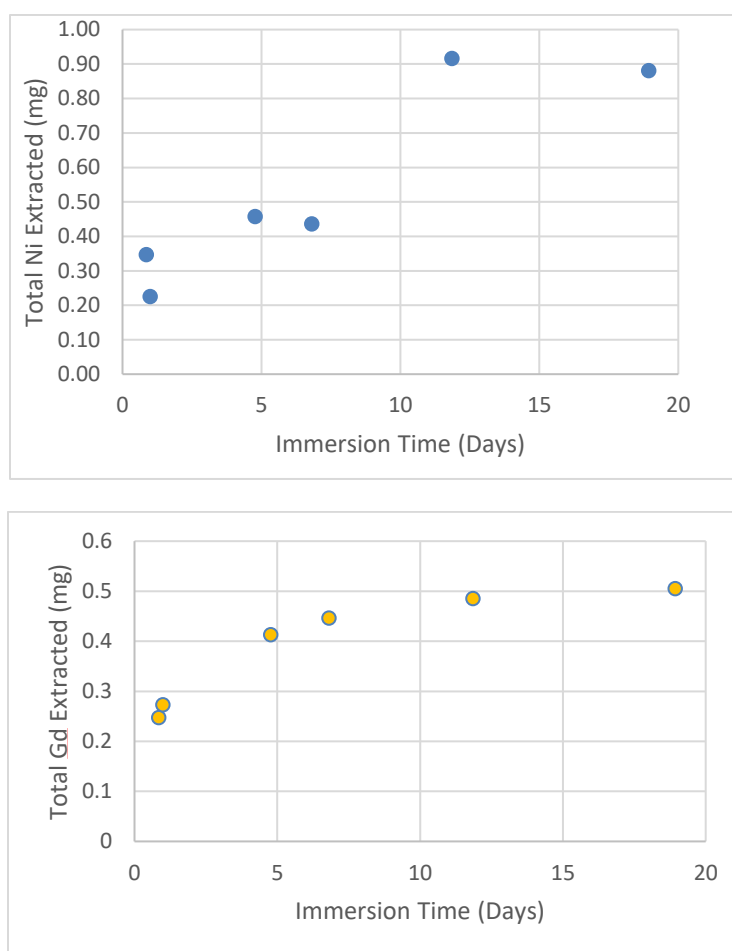


**Figure 5.** Total Ni and Gd extracted versus time for the M327 specimen during acid pickling.

Changes in mass measured gravimetrically did not follow a discernable trend over time for either alloy, possibly due to precipitation of various metal chlorides and hydroxides on the specimen surface, very

## Idaho National Laboratory

Neutron Absorber Material Corrosion  
Testing Report

Identifier:

Revision: 0

Effective Date: 09/17/2021

Page 18 of 51

apparent in the case of M326. Figure 6 shows images of the specimens after exposure. The M326 specimens shows significant coloration on the surface while M327 is relatively devoid of staining.

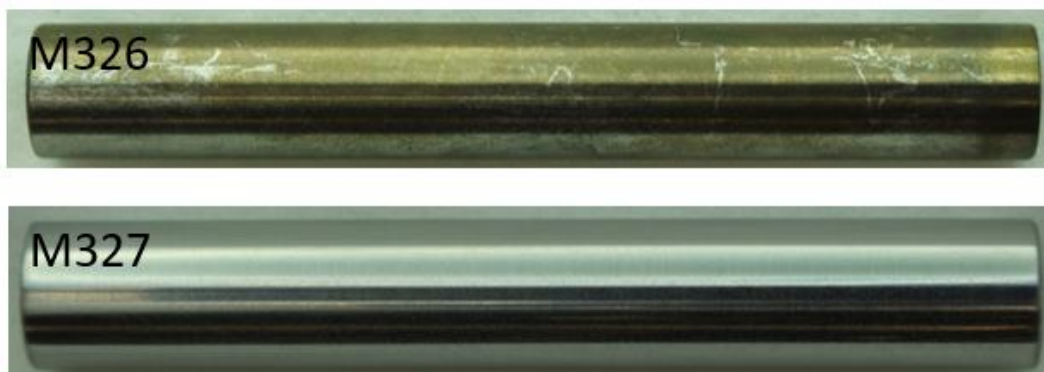


**Figure 6.** Images of specimens after acid pickling in 1.0 M HCl for 42 days.

Optical microscopy was used to examine the specimens after testing with examples shown in Figure 7. Both specimens show the typical secondary phase attack. M326 damage appears more extensive with pits more connected. An analysis of both specimens for the secondary phase distribution would be needed to make additional use of this data for assessment.

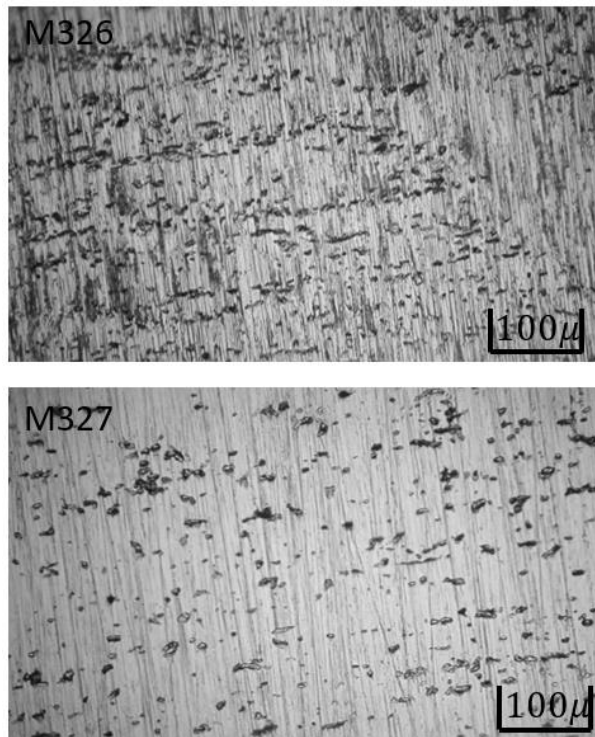


**Figure 7.** Optical microscopy images of M326 (top) and M327 (bottom) after acid pickling in 1.0 M HCl for 42 days.

## Neutron Absorber Material Corrosion Testing Report

Identifier:

Revision: 0

Effective Date: 09/17/2021

Page 19 of 51

Figure 8 shows images of M326 and M327 after pickling experiments. Only the M326 shows definite color due to ions dissolved in solution. The green color is from dissolved nickel and chromium ions.

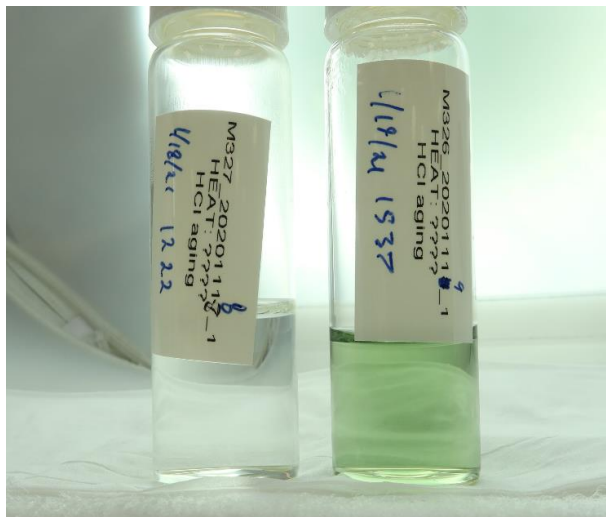


**Figure 8.** Solutions retained from pickling M327 (left) and M326 (right).

### 3.1.2 CPP testing of acid pickled ANA

After pickling, ANA specimens were examined with CPP testing to assess how removing the gadolinide phase affects the curves. Figures 9-10 show CPP curves in 0.1 M HCl for M327 and M326 after pickling with as polished results provided for comparison. In both cases, the curves for pickled specimens are lower in current, supporting the idea that the current observed across passive range is due to the secondary phase corrosion. Note that the  $E_{rp}$  (sharp point at low current on the return sweep) shifts positive for the pickled specimens, another indication of improving corrosion characteristics upon removing the secondary phases. The curve for M327 (and M326 to some extent) resembles that of Alloy 22 [15].

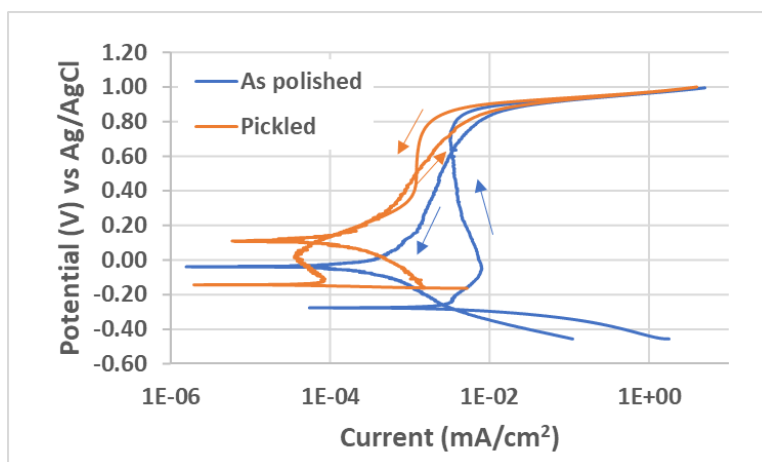


**Figure 9.** CPP curves for M327 in 0.1 M HCl with and without acid pickling.

## Neutron Absorber Material Corrosion Testing Report

Identifier:

Revision: 0

Effective Date: 09/17/2021

Page 20 of 51

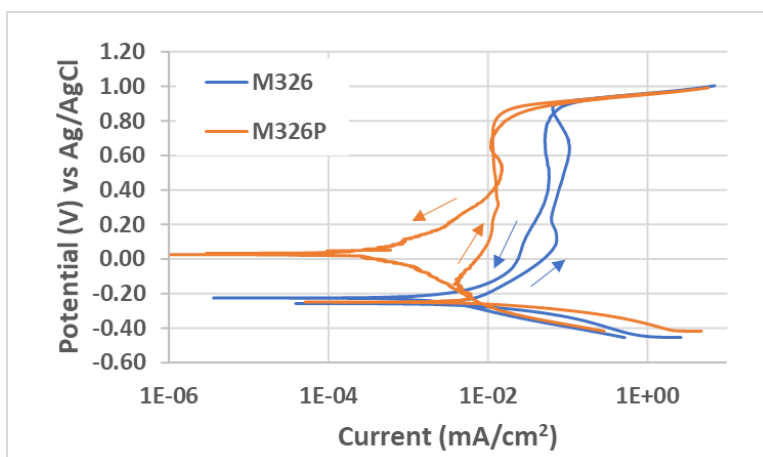


**Figure 10.** CPP curves for M326 in 0.1 M HCl with and without acid pickling.

Similar tests were performed for acid pickled specimens in seawater, shown in Figures 11-12. It is interesting that for M327 (Figure 11), there was not as significant a difference in the forward curve but a bit greater difference on the return sweep. There is a shift in  $E_{rp}$ , but it is not nearly as great (or as positive) as observed in 0.1 M HCl. In seawater, we suspect that the secondary phase dissolves much slower in the passive region (supported by the current for as polished specimens in Figure 9 vs Figure 11). Therefore, the differences in current are less for pickled vs as polished. For M326 in Figure 12, the pickled specimen shows much lower current in both directions, with current being significantly greater than the as polished M327.

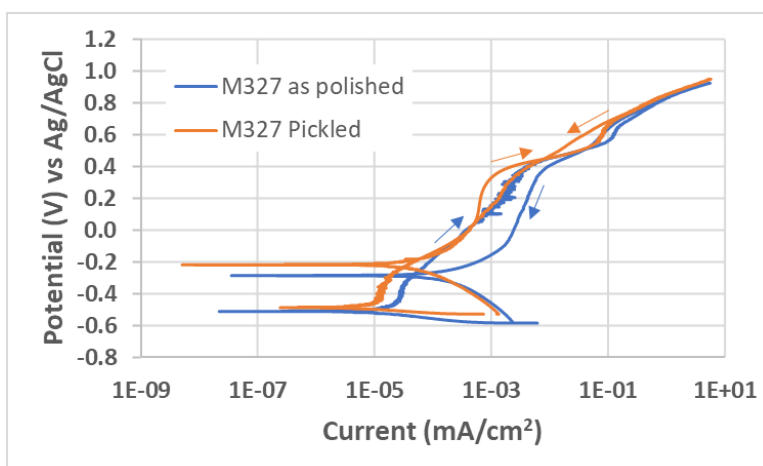


**Figure 11.** CPP curves for M327 in seawater with and without acid pickling.

For M326, a greater difference was observed for the pickled specimen which appears to be from an increased current for the as polished specimen, where the pickled specimen had only a slightly higher current than M327 (Figure 11).

## Neutron Absorber Material Corrosion Testing Report

Identifier:

Revision: 0

Effective Date: 09/17/2021

Page 21 of 51

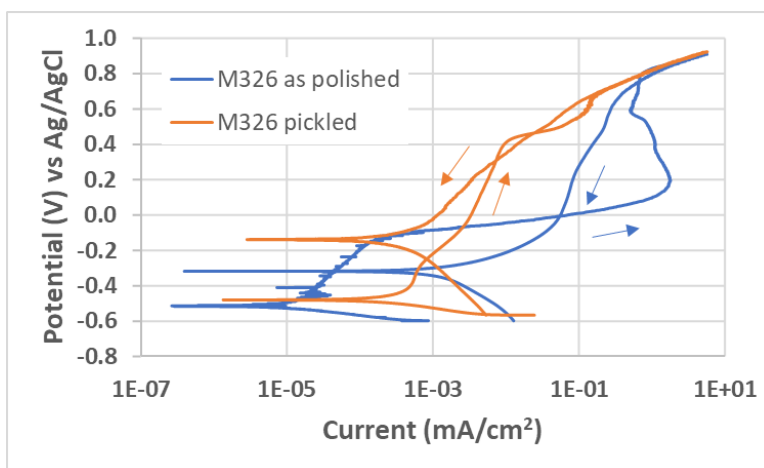


**Figure 12.** CPP curves for M326 in seawater with and without acid pickling.

Figure 13-14 shows  $E_{\text{corr}}$  curves taken before testing for pickled and as polished specimens in 0.1 HCl and seawater respectively. Note that in 0.1 M HCl, the pickled specimens show a significant positive shift and are similar to Alloy 22 (C22). In general, positive shifts in  $E_{\text{corr}}$  are indications of improved corrosion resistance. For seawater, the curves are smooth, however are shifted negative compared to the as polished specimens.  $E_{\text{corr}}$  is the measured rest potential of specimens in the environment, defined by the balance point between possible cathode and anodic reactions. The corrosion of gadolinides at  $E_{\text{corr}}$  in seawater for the as polished specimens is the likely reason for this inversion of trend.

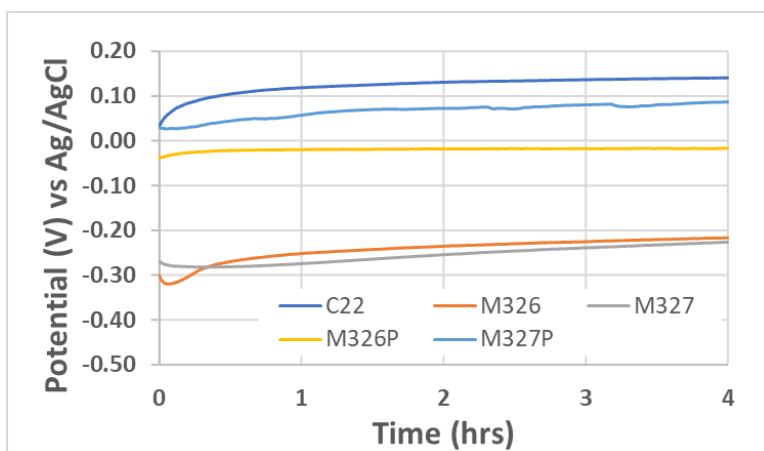


**Figure 13.**  $E_{\text{corr}}$  of Ni alloys in 0.1 M HCl with and without pickling.

## Neutron Absorber Material Corrosion Testing Report

Identifier:

Revision: 0

Effective Date: 09/17/2021

Page 22 of 51

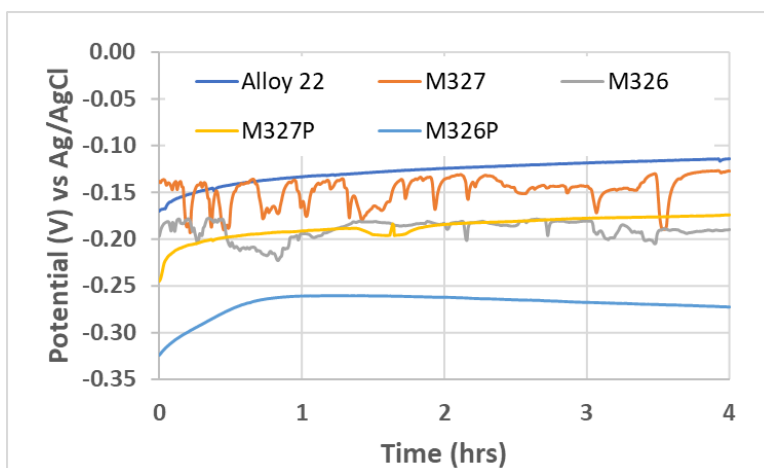


**Figure 14.**  $E_{\text{corr}}$  of Ni alloys in seawater with and without pickling.

Figure 15 shows a cross-sectional SEM images for M326 and M327 specimens after pickling and CPP testing in 0.1 M HCl (Figure 9-10). On the images, the curved surface to the right is the exposed surface. Bright regions are gadolinide particles and dark regions are presumed to be areas where gadolinides have been dissolved. For M326, several dark regions exist near the exposed edge of the specimen. In some cases, these appear to be deep into the specimen. The M327 specimen appears to show only loss of gadolinides close to the surface. A quantitative assessment of these images has not yet been performed, but generally this appears to support that the secondary phase is removed deep into the specimen for M326 and not M327, as discussed in Section 3.1.1.



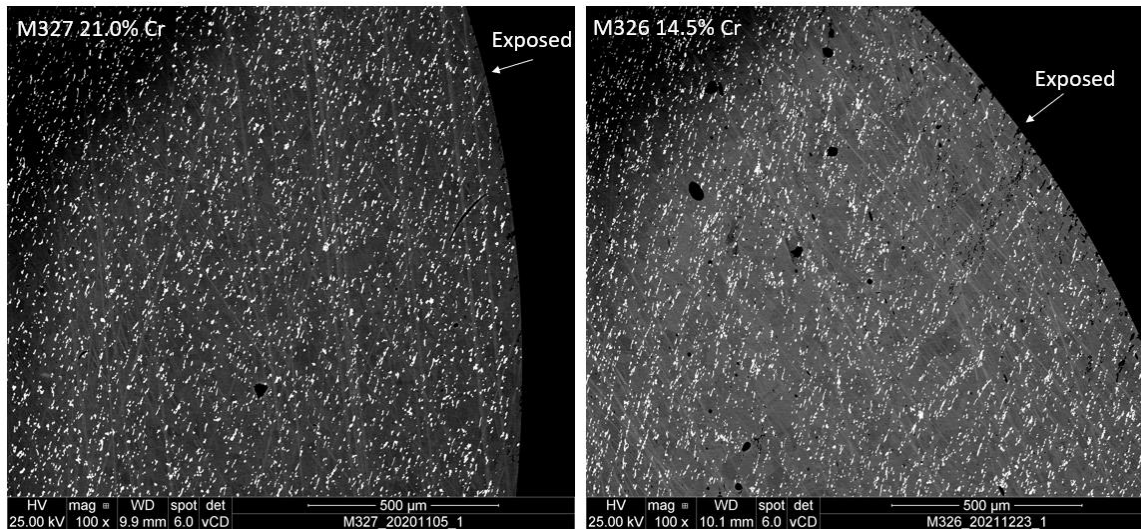


**Figure 15.** SEM images (backscatter mode) of the cross-section of M327 and M326 specimens after pickling and CPP testing in 0.1 M HCl.

Figure 16 shows SEM images of the exposed surface of ANA specimens (same as in Figure 15). These images show small pits which have been reported for ANA previously [16]. These small pits are where gadolinide particles had dissolved.

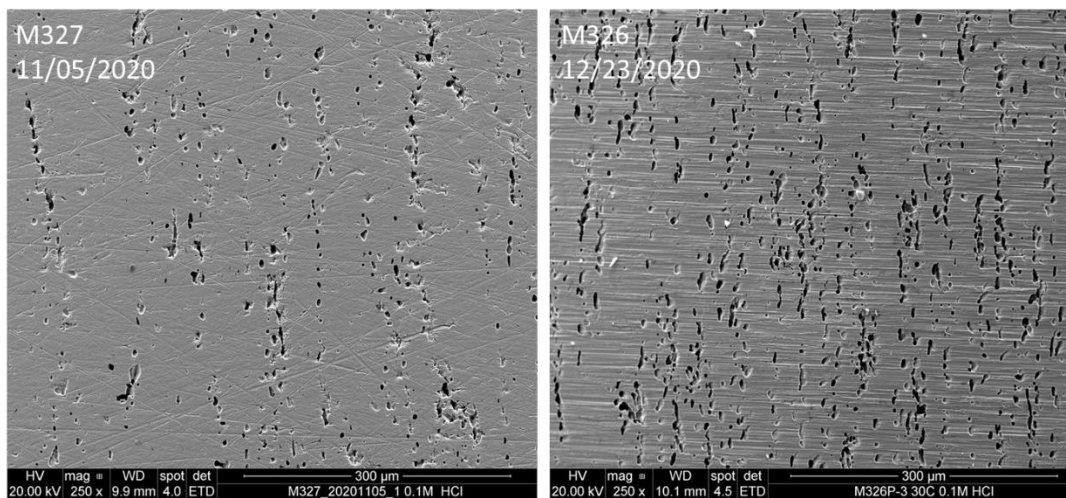


**Figure 16.** SEM images of M327 and M326 specimens after pickling and CPP testing in 0.1 M HCl.

### 3.1.3 PS testing of ANA

PS tests were performed for ANA specimens as well as Alloy 22 and Alloy C-4 as benchmarks. These tests were performed at 0.2 V vs Ag/AgCl reference electrode, which is considered an accelerated condition based on previous corrosion potential ( $E_{\text{corr}}$ ) measurements [15] and results presented in Figure 14. Thus, these results should be considered as good comparisons but not necessarily indicative of actual



## Neutron Absorber Material Corrosion Testing Report

Identifier:

Revision: 0

Effective Date: 09/17/2021

Page 24 of 51

performance. Figure 17 shows a set of PS curves for M326, M327, C-4 and Alloy 22. The two benchmark alloys show approximately the same current profiles with Alloy 22 being just slightly lower than C-4.

This suggests that for this condition the additional Cr in Alloy 22 is not providing any significant benefit.

Both ANA specimens show greater current that decreases over time. The current for M327 is about 1.5 orders of magnitude greater than the benchmark alloys and about 2 orders of magnitude lower than M326.

This suggests that the additional chromium (14.7% vs 21%) is quite beneficial.

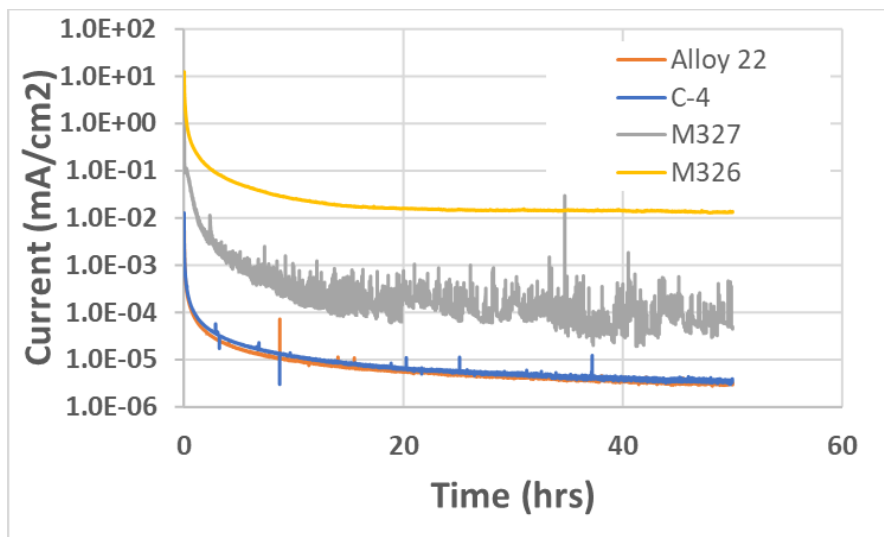


**Figure 17.** Current vs time curves for M326, M327, Alloy 22 and Alloy C-4 in seawater.

The benefit of additional Cr in ANA was further considered by examining available ANA materials from previous efforts. Figure 18 shows a series of curves from these tests including the same curves from M327 and M326 shown in Figure 17. Unfortunately, there were not any alloys with Cr above 16.75% (except M327), so this analysis is limited. Also note that M322 has 2.38% Gd and D5-8235 has 1.89% Gd. In general, the current drops with increasing Cr content, approximately 0.5 orders of magnitude between M326 (14.7% Cr) and D5-8235 (16.75% Cr). This current was converted to a corrosion rate (assuming general corrosion) using ASTM G102 and plotted versus Cr content in Figure 19 [13]. The two red points are the benchmark alloys showing the lowest corrosion rates. The highest rate was for M322 (2.38% Gd). Although it would be helpful to have a better distribution of Cr composition, the rates for ANA decrease with Cr composition.

## Neutron Absorber Material Corrosion Testing Report

Identifier:

Revision: 0

Effective Date: 09/17/2021

Page 25 of 51

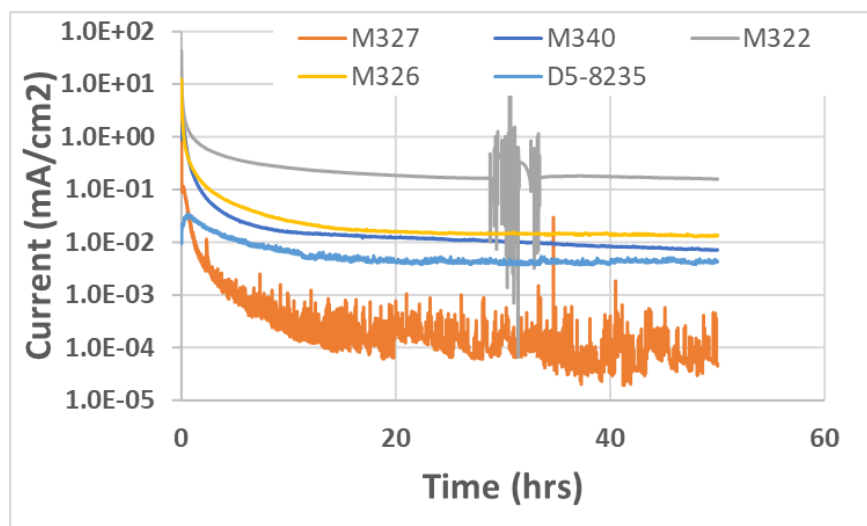


**Figure 18.** Current vs. time curves for various ANA specimens in seawater.

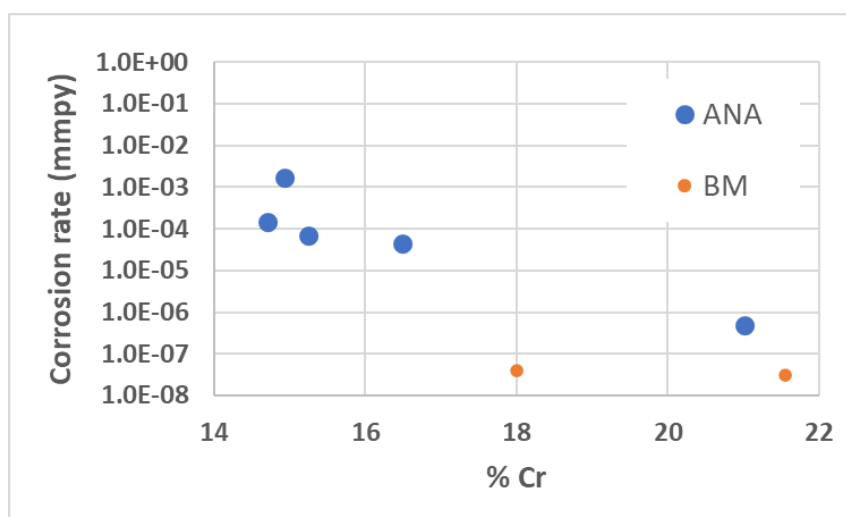


**Figure 19.** Plots of corrosion rates calculated from the final current data point from PS tests in seawater for ANA (blue) and benchmark alloys (red).

Additional data was collected from the PS test sequence as shown in Table 3. The benchmark alloys showed almost no weight loss from experiments. The weight loss trends were similar to the electrochemical data but is not considered a great indicator as chemical descaling (beyond sonication in water) to remove corrosion products and salt films was not performed. The total charge for the experiment was calculated using the integration function in the potentiostat software and scaled to exposed surface area. The charge can be related to the amount of corrosion that occurred in the specimen, assuming no other electrochemical reaction was occurring (unlikely). The M322 specimen shows the most charge and values decrease with Cr content and as expected follows the trends for current data in

## Idaho National Laboratory

<b>Neutron Absorber Material Corrosion Testing Report</b>	Identifier: Revision: 0 Effective Date: 09/17/2021
---	--

	Page 26 of 51
--	---------------

Figure 18. The corrosion rates were determined before and after the PS tests using LPR. The LPR determined rates before testing generally follow the level of Cr but not as dramatically as the PS current. The rates after testing were greater for all ANA specimens, indicating that the new surface produced from gadolinide dissolution could be considered less passive as the original surface. This could be from insufficient time for passivation to occur after being in an accelerated corrosion state. The values for M327 are the exception, where the values are essentially the same. This is also the case for the benchmark alloys, another indicator that M327 behave more like the benchmark alloys than the lower Cr ANA specimens.

**Table 3.** Data collected from the PS test sequences.

Alloy	% Cr	Potential (V)	Weight loss (g/cm <sup>2</sup> )	Total Charge (C/cm <sup>2</sup> )	PS CR (mmpy)	LPR CR (mmpy)	LPR CR Post-test (mmpy)
M322	14.93	0.2	1.77E-02	53.26	1.75E-03	6.47E-05	7.76E-02
M326	14.71	0.2	2.36E-03	7.67	1.47E-04	4.23E-05	1.12E-02
M340SR	15.25	0.2	1.64E-03	5.25	6.76E-05	4.21E-05	5.01E-03
D5-8235	16.49	0.2	3.42E-04	1.17	4.40E-05	4.12E-06	2.32E-03
M327	21.01	0.2	1.08E-04	0.31	4.84E-07	5.03E-05	5.21E-05
C4	18	0.2	1.48E-06	0.003	4.04E-08	9.09E-06	2.68E-05
C22	21.55	0.2	2.61E-06	0.002	3.05E-08	7.65E-06	3.49E-06
M326	14.71	0	6.3E-05	0.223	3.38E-06	6.02E-05	1.83E-04

A test was also performed for M326 at 0 V as shown in Figure 20. This voltage is closer but still positive of the range of  $E_{\text{corr}}$  values measured for acid pickled specimens (Figure 14)[15]. This experiment showed much lower charge and the corrosion rate based on the PS current was almost 2 orders of magnitude lower. The LPR determined corrosion rate after the test was also lower, suggesting less damage to the specimen. This agrees with the very low weight loss observed. SEM analysis of the specimen held at 0 V indicates that the gadolinide phase is mostly intact (Figure 23).

## Neutron Absorber Material Corrosion Testing Report

Identifier:

Revision: 0

Effective Date: 09/17/2021

Page 27 of 51

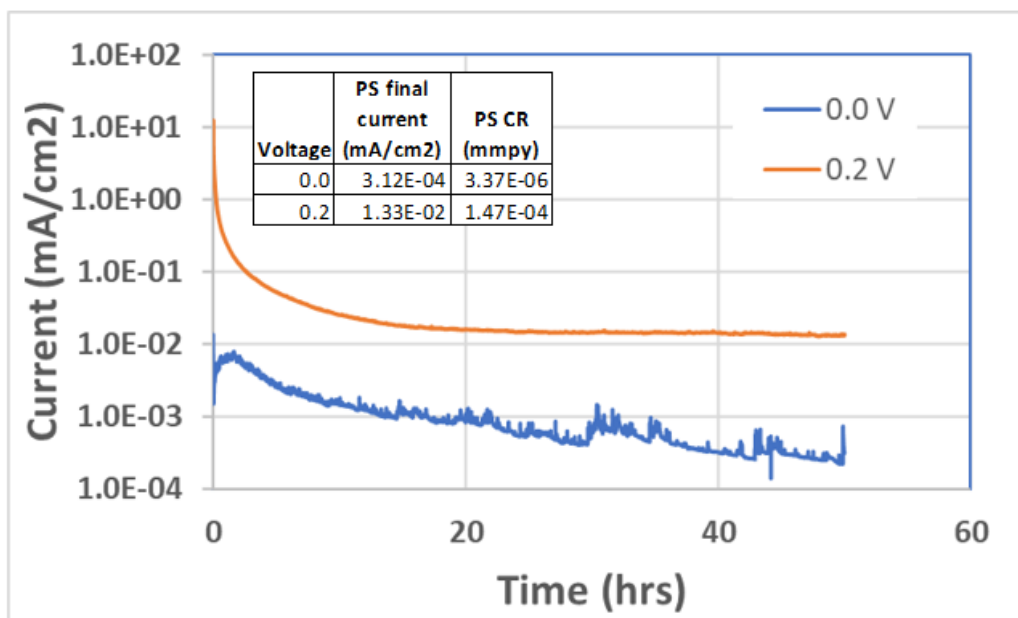


**Figure 20.** PS tests of M326 at 0 V vs Ag/AgCl in seawater. Inset shows the final current and calculated corrosion rate.

Figure 21 shows images of M326 specimen immediately after a PS test at 0.2 V. After testing, ANA specimens were found to have a white coating and black particles on the surface as shown in the top image. This deposit is easily removed in the cleaning procedure (only sonication in water) to reveal a specimen with many small pits on the surface as has been observed previously [15]. The white deposit could be the result of sulfate and/or fluoride ions present in seawater resulting in precipitation with dissolving metal ions. Figure 22 shows an image of the M322 specimen after the PS test before removing from the corrosion vessel. This specimen showed the greatest corrosion of all specimens (with the highest Gd content at 2.38%) and as a result has significant amounts of the white flocculent precipitate. In this test the precipitate appeared to largely fall off during removal. It is known that rare earth elements such as Gd have limited solubility at neutral pH values with sulfate and fluoride present [16]. Gadolinium sulfate is sparingly soluble at 3 g per 100 mL while gadolinium fluoride is very insoluble with a solubility product of  $6.7 \times 10^{-17}$ . White precipitate was collected for x-ray diffraction (XRD) analysis, but no database matches were obtained.

<b>Neutron Absorber Material Corrosion Testing Report</b>	Identifier:	
	Revision:	0
	Effective Date:	09/17/2021

Page 28 of 51

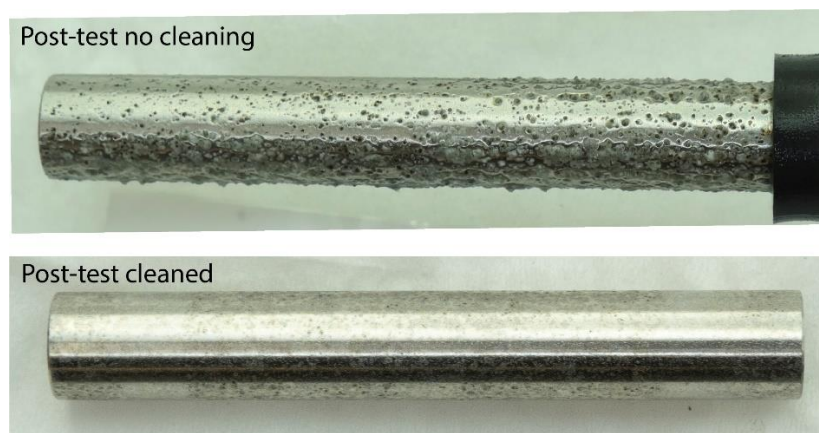


**Figure 21.** Images of M326 specimen immediately after testing and after cleaning specimen.



**Figure 22.** Image of M322 after PS testing before removal from the test vessel showing a significant amount of white corrosion product.

Figure 23 presents two SEM (backscatter mode) images of specimens tested in seawater. On the left image, an M327 specimen was tested at 0.2 V shows that despite a long test period (50 hrs), not all gadolinides (showing up as bright areas) have dissolved (areas that are dark) in seawater. The image on the right shows M326 poised at a more positive potential in seawater, showing very little dissolution of gadolinides, which agrees with the current curve in Figure 20.

## Neutron Absorber Material Corrosion Testing Report

Identifier:

Revision: 0

Effective Date: 09/17/2021

Page 29 of 51

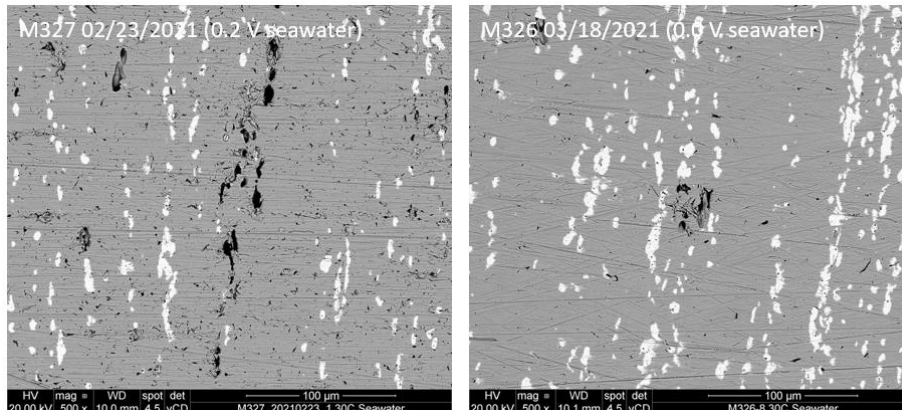


**Figure 23.** SEM images (backscatter mode) for PS tested specimens in seawater. Left: M327 at 0.2 V and Right: M326 at 0.0 V.

### 3.2 PS testing of 304L and 316L

PS tests were performed at various potentials just positive of the measured  $E_{\text{corr}}$  values for benchmark stainless steel specimens 304L and 316L in seawater. These specimens were used as surrogates, as a limited amount of Grade A BSS specimens remain and these tests, due to the incurred damage, often prevent reuse. These tests can be useful from a bounding perspective, in that these would represent the best performance and that B addition would only diminish from these results. Recent results also showed that BSS specimens performed similar to 304L [15]. Figure 24 shows three curves for 304L at 0.0, 0.1 and 0.2 V, shown in log scale due to range of data observed. Figure 25 shows the associated images post-test. At 0.0 V, there were small current transients present but the baseline current was very low. For 0.1 and 0.2 V, very large current and catastrophic damage was observed as shown in Figure 25. The fact that the current increases 4 orders of magnitude for only 0.1 V of potential highlights the sensitivity of stainless steel to pitting corrosion in chloride environments. Also note that the  $E_{\text{pit}}$  value from FY2020 testing was 0.156 V and 0.107 V [15], which is positive of 0.1 V but one would assume the point of minimal stability (pit initiation without passivation) is somewhere between 0.0 and 0.1 V.

## Neutron Absorber Material Corrosion Testing Report

Identifier:

Revision: 0

Effective Date: 09/17/2021

Page 30 of 51

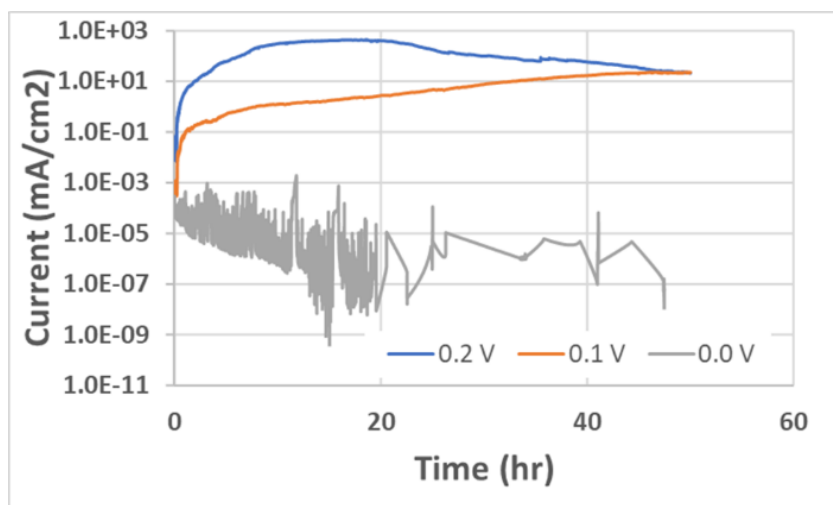


**Figure 24.** Potentiostatic tests for 304L in seawater at 0, 0.1 and 0.2 V vs Ag/AgCl.

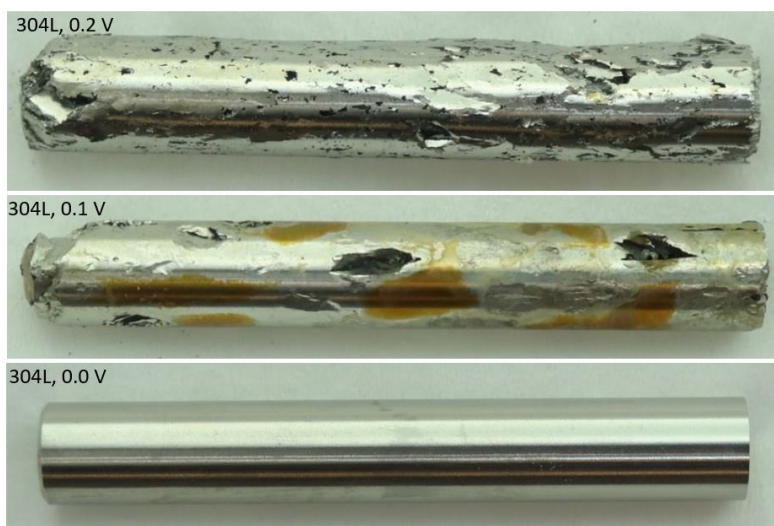


**Figure 25.** Images of 304L specimens from Figure 1.

Similar tests were performed for 316L at 0.1 and 0.2 V as shown in Figure 26 and associated post-test images are shown in Figure 27. For 0.1 V, the results were very similar to those observed for 304L at 0.0 V with metastable pit initiation and passivation. At 0.2 V, significant corrosion was observed at 0.1 and 0.2 V for 304L. For 316L, there was an initiation period of over an hour at the start of the test. In CPP tests presented in the FY2020 report, the  $E_{\text{pit}}$  values were 0.365 V and 0.348 V [15], significantly higher than 0.2 V. This illustrates that pitting corrosion is a challenge to evaluate using only one method and that  $E_{\text{pit}}$  is useful for comparison purposes, but the actual potential of stability to pitting is more negative due to the latent or dormant nature of corrosion.

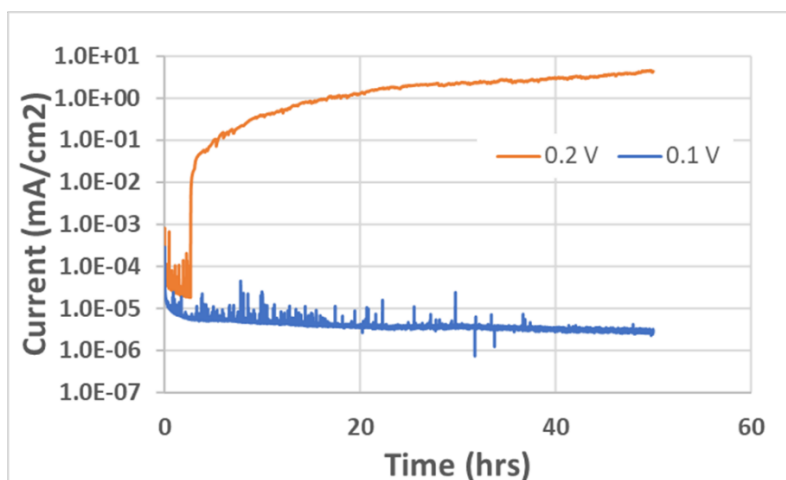


**Figure 26.** PS tests performed for 316L at 0.1 and 0.2 V vs Ag/AgCl.

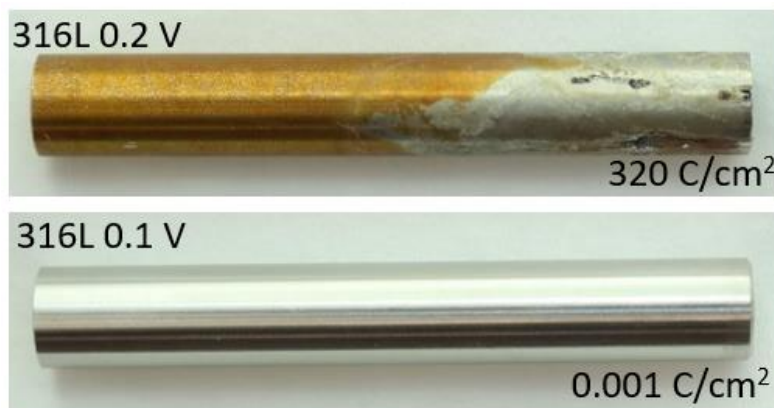


**Figure 27.** Images of 304L specimens from Figure 3.

Figure 28 shows the  $E_{\text{corr}}$  data for 304L and 316L for two of the tests above. For 304L, curves tended to slowly increase during the test and a rate of 6.28 mV/hr was determined for the data in Figure 28 after the initial ~40 min equilibration period. The  $E_{\text{corr}}$  values for 316L tended to be slightly more positive and showed more steady behavior. Both curves do show negative spikes in voltage which are indicative of pitting initiation/passivation.



## Neutron Absorber Material Corrosion Testing Report

Identifier:

Revision: 0

Effective Date: 09/17/2021

Page 32 of 51

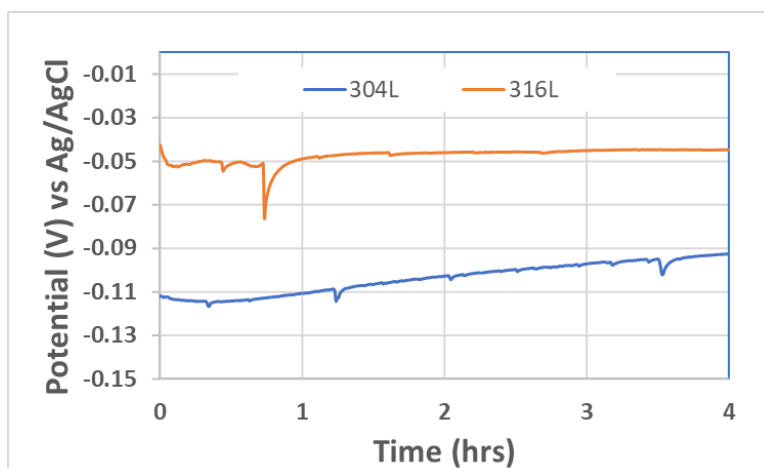


**Figure 28.**  $E_{\text{corr}}$  values for 304L and 316L in seawater.

The data shown above provides context to what was observed for BSS specimens in previous testing [14]. Significant damage was observed for 304B6 specimens at potentials that had much lower effect on ANA specimens. Put into the context of the data shown above, the sharp drop off in performance with potential appears more of a property of the base metal formulation (Type 304 SS) than boron addition alone, which serves to decrease performance further. While it has been documented that B does tie up Cr [17], the challenge to being suitable for an environment derived from seawater appears to lie in the stability of the base formulation. For Type 304 formulations, pitting can be expected somewhere between 0 and 0.1 V vs Ag/AgCl (Figure 24). It appears that 316L increases the threshold at least 0.1 V more positive. Figure 28 shows that while there is a margin between  $E_{\text{corr}}$  and these breakdown voltages, it is not a wide margin and for 304L we do not see a stable voltage being reached in the 4-hr window. It is also suspected that increases in temperature above 30 °C will significantly decrease or eliminate the stability gap. Given that all Grade A (powder metallurgy) commercial BSS alloys (past and present) are based on 304L, it stands to reason that they will not be suitable for seawater. The only known BSS alloy was based on Type 316 was a Grade B (ingot metallurgy), which shows significantly degraded performance to Grade A [18].

### 3.4 Cold-sprayed C22Gd specimens

This section describes corrosion testing of specimens produced by SNL using C22Gd powder purchased in an order from Haynes International. The results from this work are ongoing and will be updated when post-test analysis becomes available.

#### 3.4.1 Pre-test analysis of ANA coatings

## Neutron Absorber Material Corrosion Testing Report

Identifier:

Revision: 0

Effective Date: 09/17/2021

Page 33 of 51

Analysis of specimens after spraying was performed at SNL and communicated through a short report [19]. This section provides images and data from that analysis. Figure 29 shows images of the specimens sent to INL for testing.

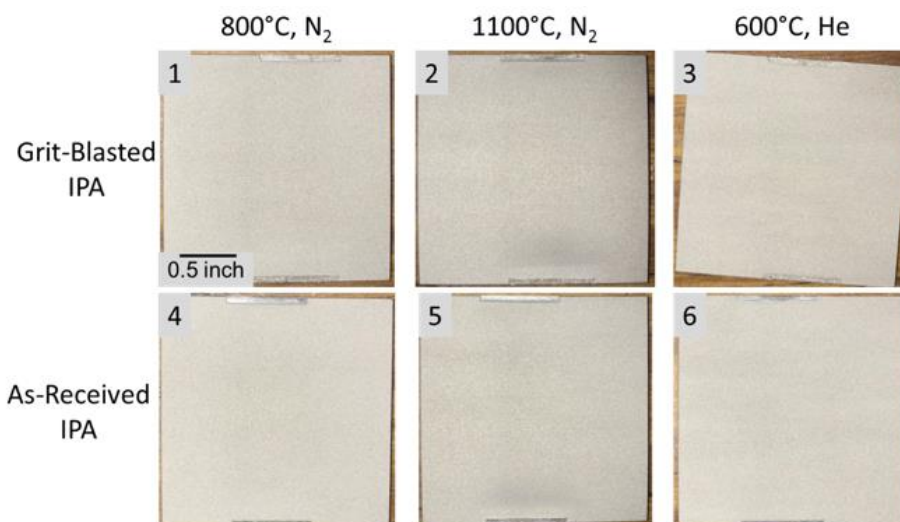


**Figure 29.** Optical images of specimens coated by cold spray of C22Gd alloy.

SNL performed cross-sectional analysis of coatings using the same conditions used to produce the specimens as shown in Figure 30. SEM images show darker areas that can be ascribed to porosity in the coatings. Image analysis was used to estimate the density of the specimens presented on the images, which all exceed 96%.



**Figure 30.** SEM images of the cross-section of C22Gd coatings.

Figure 31 shows SEM images and corresponding energy dispersive spectroscopy (EDS) analysis of a specimen coated at 1100 °C. This condition was chosen as the most likely to show secondary phase precipitation. The backscatter image in the upper right shows some differences which could be density related. In the upper right image, the defined borders are particle boundaries which agrees with the powder particle size (~25 µm). Wrought material with defined gadolinide particles registered those as

**Neutron Absorber Material Corrosion  
Testing Report**

Identifier:

Revision: 0

Effective Date: 09/17/2021

Page 34 of 51

brighter areas in SEM backscatter images [11]. However, EDS imaging did not pick up any strong correlation for these bright areas and abundance of Gd. While there is some variation of Gd among particles, there is not a strong correlation. This suggests that the gadolinide phase is highly dispersed in the specimens.

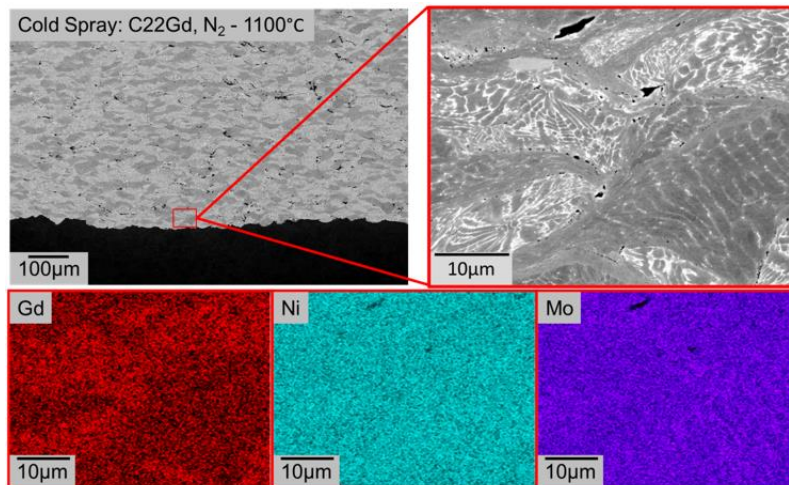


**Figure 31.** SEM backscatter imaging and EDS analysis of the chemical distribution for a small area of the surface.

### 3.4.2 CPP testing of ANA coatings

CPP tests were performed using the flat specimen holder in seawater. Figure 32 show  $E_{\text{corr}}$  plots for materials at the three conditions used for coating as well as Alloy 22 from previous testing. The coated specimens all showed hints of pit initiation but not nearly as pronounced as shown in Figure 14 for wrought ANA specimens.

## Neutron Absorber Material Corrosion Testing Report

Identifier:

Revision: 0

Effective Date: 09/17/2021

Page 35 of 51

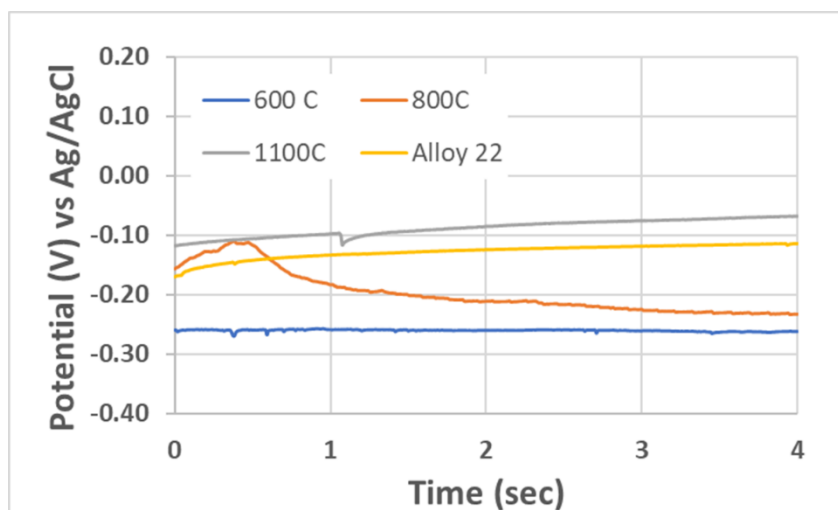


**Figure 32.**  $E_{\text{corr}}$  measurements performed in seawater before CPP testing. Alloy 22 from previous tests was included for reference.

Figure 33 shows CPP curves for the three materials as well as Alloy 22 and M327 for reference. The C22Gd coated at the two lower temperatures shows current increase starting around -0.3 V as is common for ANA but is certainly much greater than M327. Interesting, the C22Gd coated at the highest temperature had a delayed increase in current to ~-0.25 V, where it increased rapidly to near that of the lower temperature specimens. On the return sweep, there was hysteresis observed, with current remaining at high levels until approximately -0.3 V. Overall, the 1100 °C specimen showed lower current and charge as shown in Table 4.

## Neutron Absorber Material Corrosion Testing Report

Identifier:

Revision: 0

Effective Date: 09/17/2021

Page 36 of 51

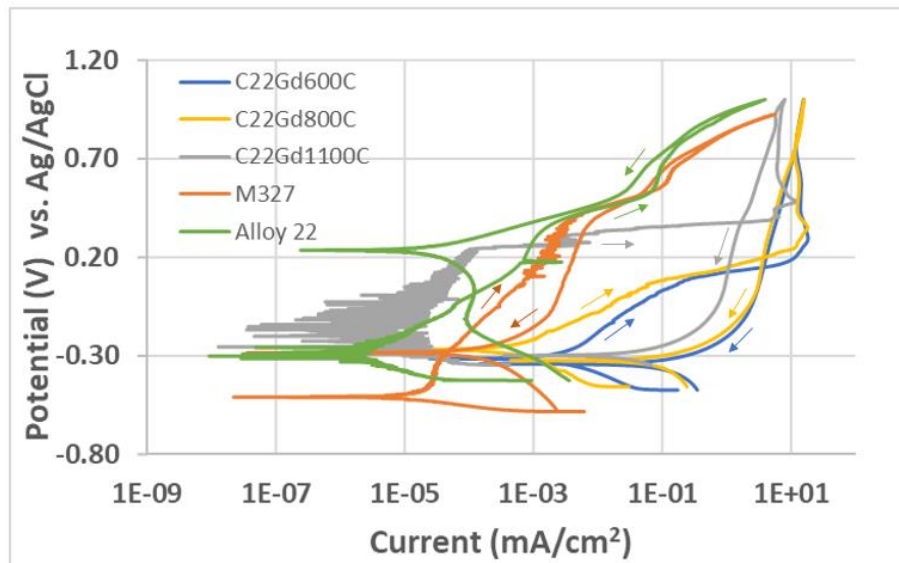


**Figure 33.** CPP tests performed in seawater for C22Gd coatings with M327 and Alloy 22 added for reference.

**Table 4.** Data obtained from CPP curves for C22Gd coatings.

Specimen	Charge (C/cm <sup>2</sup> )	Peak Current (mA/cm <sup>2</sup> )
<b>C22Gd 600</b>	123.095	18.427
<b>C22Gd 800</b>	112.788	18.073
<b>C22Gd 1100</b>	44.388	11.513

Figure 34 shows photographs of the exposed areas after CPP testing. For the specimens coated at the two lower temperatures, there are darker (red-brown) spots on the surface that appear to be pits. Closer examination with a microscope was inconclusive if these were pits or stains due to the rough nature of the coatings. The 1100°C specimen showed a more uniform grey appearance after testing. Note that the coatings have a high degree of surface roughness, making it a challenge to capture optical microscopy images on a conventional microscope. SEM images were not yet available for this report and will be added in a revision to this document.

## Neutron Absorber Material Corrosion Testing Report

Identifier:

Revision: 0

Effective Date: 09/17/2021

Page 37 of 51

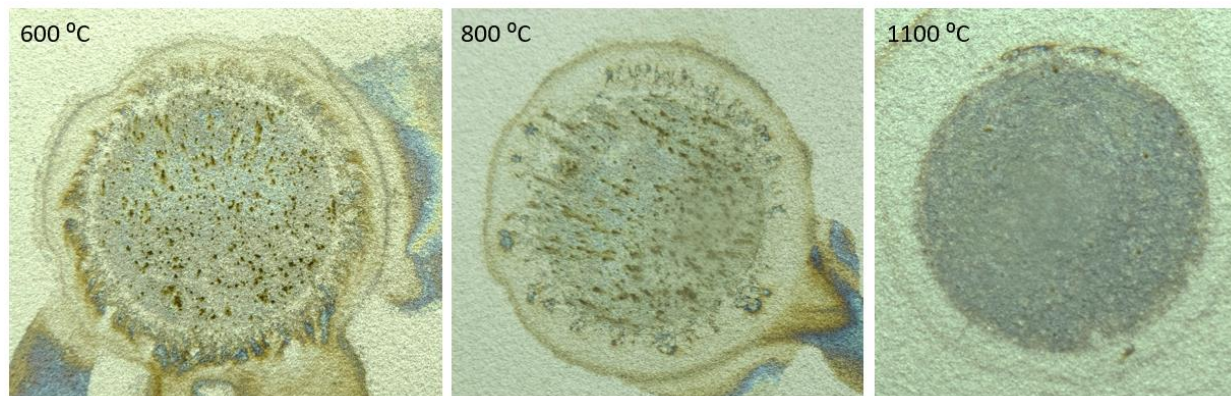


**Figure 34.** Photographs of specimens after CPP testing in seawater.

### 3.4.3 PS testing of ANA coatings

Figure 35 shows PS curves for C22Gd coatings held at 0.2 V vs Ag/AgCl. The specimens at low temperature show greater initial current which is sustained at a fairly high level for most of the test. All specimens show almost an order of magnitude drop in current during the test, with the 600 °C specimen falling to the lowest current and continually dropping. The 1100 °C specimen showed lower current initially but the current drop comes later than observed for the 600 °C specimen. The 800 °C specimen sustains high current through most of the test, dropping in current just before the test ends. Data obtained from the PS curves is summarized in Table 5. The final current was used for calculating the corrosion rate, which is significantly higher than for wrought ANA materials.

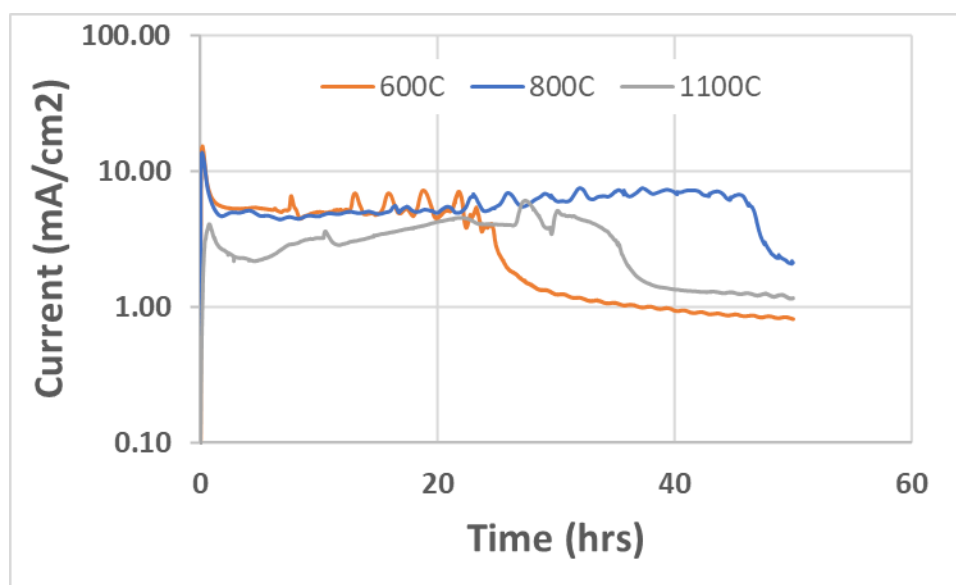


**Figure 35.** PS curves for C22Gd coatings in seawater at 0.2 V vs Ag/AgCl.



## Neutron Absorber Material Corrosion Testing Report

Identifier:

Revision: 0

Effective Date: 09/17/2021

Page 38 of 51

**Table 5.** Charge and current values obtained from PS tests in Figure 35.

Specimen	Charge (C/cm <sup>2</sup> )	Peak current (mA/cm <sup>2</sup> )	Final Current (mA/cm <sup>2</sup> )	PS CR (mmpy)
600 C	583.84	15.27	8.16E-01	8.51E-03
800 C	1014.11	13.68	2.12E+00	2.21E-02
1100 C	532.05	6.08	1.16E+00	1.21E-02

Figure 36 shows images of the specimens after PS testing shown in Figure 35. Significant changes to the surface are evident in all specimens. The roughness of the as coated specimens make assessment a challenge, but it appears significant pitting has occurred. SEM images were not yet available for this report and will be added in a revision to this document.

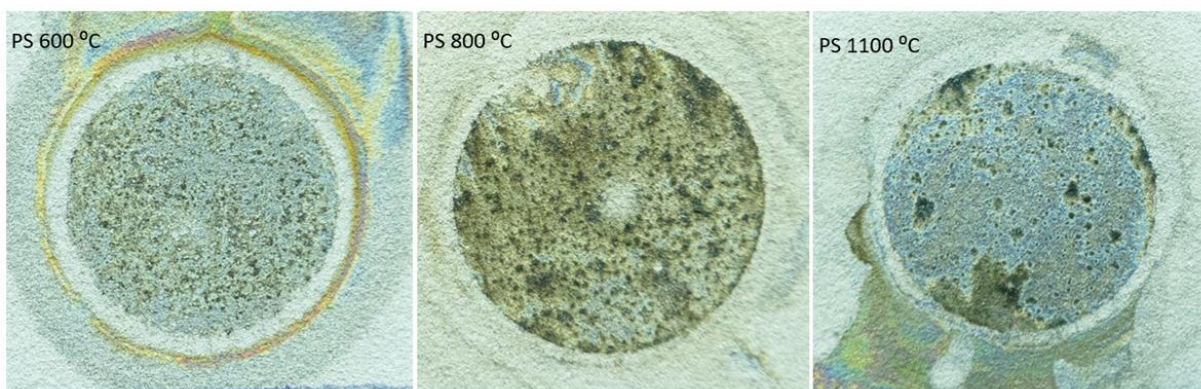


**Figure 36.** Images of specimens after PS testing.

The roughness of the as received specimens suggested that a portion of the increased current observed is related to the roughness of the as received coatings. The specimens were carefully abraded with 600 grit sandpaper to remove the coarse outer layer while attempting to avoid breaking through to the 316L base material. Figure 37 shows PS curves for as received and polished specimens as well as an M327 specimen taken using a conventional cylindrical specimen. While the polished specimen shows slightly decreased current initially, it eventually reaches and exceeds that of the as received specimen. Figure 37 also shows the great decrease in performance over the M327 specimen, where current is 4 to 5 orders of magnitude lower.

## Neutron Absorber Material Corrosion Testing Report

Identifier:

Revision: 0

Effective Date: 09/17/2021

Page 39 of 51

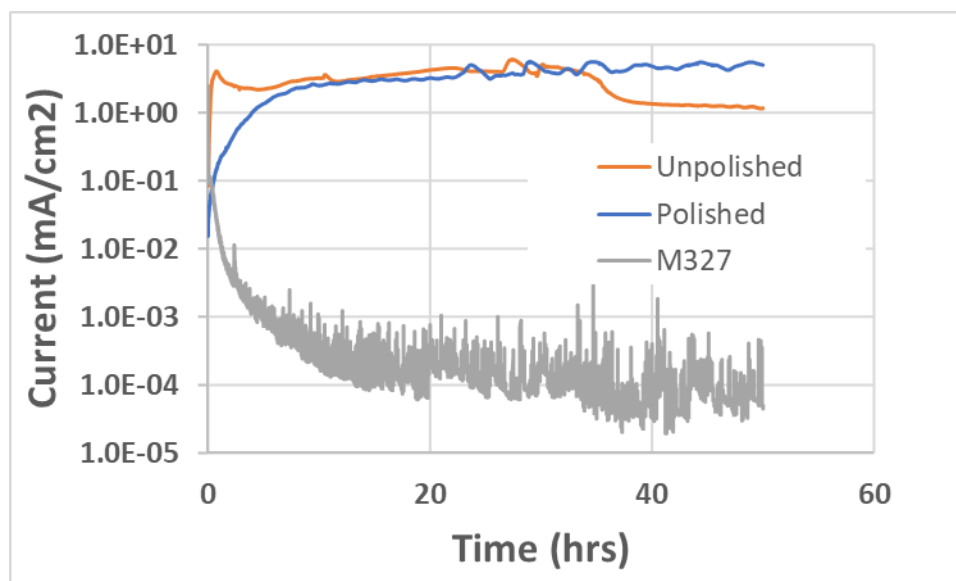


**Figure 37.** PS curves for unpolished and polished 1100 °C C22Gd coatings with M327 presented for reference.

Figure 38 shows an image of the 1100 °C C22Gd specimen tested in Figure 37, where pitting and crevice attack are observed around almost the entire circumference. Note that the M327 specimen was of the cylindrical type and no crevice was imposed. However, it is unlikely the crevice contributed that significantly to the decreased performance as pits are present away from the gasket edge. SEM images were not yet available for this report and will be added in a revision to this document.



**Figure 38.** Image of polished C22Gd (1100°C) specimen after PS testing (Figure 37).

### 3.4.4 General corrosion of ANA coatings

General corrosion rates were calculated based using LPR measurements performed before CPP and PS tests. The average of the three LPR sweeps is presented in Table 6. The C22Gd specimen coated at 1100



## Idaho National Laboratory

<b>Neutron Absorber Material Corrosion Testing Report</b>	Identifier:
	Revision: 0
	Effective Date: 09/17/2021

Identifier:		
Revision: 0		
Effective Date: 09/17/2021		Page 40 of 51

$^{\circ}\text{C}$  had somewhat lower rates. The rates are somewhat greater than those recorded for seawater in FY2020 testing which ranged from  $1\text{E-}5$  to  $1\text{E-}4$  mmpy for M326 and M327 for as polished ANA specimens [15].

**Table 6.** Corrosion rates and standard deviations calculated from three LPR sweeps prior to CPP and PS tests.

Test	Rate (mmpy)	Std dev (mmpy)
C22Gd 600C CPP1	1.18E-02	9.81E-04
C22Gd 600C CPP2	1.70E-03	6.46E-05
C22Gd 600C PS1	2.34E-03	3.21E-04
C22Gd 600C PS2	8.74E-04	6.39E-04
C22Gd 600C Polished PD	1.14E-03	6.68E-05
C22Gd 800C CPP1	1.77E-03	2.19E-04
C22Gd 800C CPP2	8.43E-04	6.23E-05
C22Gd 800C PS1	2.03E-03	1.09E-04
C22Gd 1100C CPP1	1.95E-05	6.83E-06
C22Gd 1100C CPP2	2.40E-05	1.87E-05
C22Gd 1100C PS 1	4.19E-04	8.86E-05
C22Gd 1100C Polished PD	4.89E-05	1.11E-05
C22Gd 1100C Polished PS	4.79E-03	8.25E-03

### 3.5 Neutron Absorber materials options

#### 3.5.1 Duplex Stainless Steels with Gd and/or B + Gd alloys

Duplex (17-22 wt.% Cr) and super-duplex (25-27 wt.% Cr) SSs have a long history of use in components for seawater service [20]. The alloy chemistry of these iron-based materials consists of a mixture of austenitic and ferritic phases with a nominal distribution of about 50% austenite and 50% ferrite. This phase distribution will vary with alloy chemistry. The super-duplex alloys need to be specified for seawater service. Three recent research papers discuss an addition of B and Gd to duplex alloys in a laboratory setting where small heats of these materials were cast and rolled into sheet [21-23]. The goal of the program was to compare these alloys to BSS used for spent nuclear fuel storage in a storage pool. Choi, et al discusses the addition of 1 wt.% Gd to a duplex alloy with a 31% ferrite and 69% austenite microstructure [21]. The material was cast and rolled to a sheet product thickness of 6mm. The chemical composition of the heat is shown in Table 7. No corrosion data was presented. The Gd was found as unidentified precipitates at the grain boundaries and inside the grains. A second paper by Choi, et al. describes the fabrication of an alloy with a much lower Gd content [22]. The test material was cast and rolled into sheet with a thickness of 3 mm. Various mechanical property measurements and microstructural features were described. The alloy microstructure, crystallographic texture, mechanical

## Idaho National Laboratory

Neutron Absorber Material Corrosion  
Testing Report

Identifier:

Revision: 0

Effective Date: 09/17/2021

Page 41 of 51

properties, and corrosion behavior were described. The phase distribution (austenite and ferrite) was not described. The corrosion current using the potentiodynamic corrosion tests, (25°C in artificial seawater per ASTM D11141-98) [11]) was reported as 0.59 – 1.06 mA/cm<sup>2</sup> (the corrosion current was not converted to a corrosion rate). These measurements were made on samples from the rolling direction, transverse direction, and the short transverse direction. For comparison, corrosion current values for various NAM and benchmark alloys in seawater are several orders of magnitude lower (0.0005 to 0.005 μA/cm<sup>2</sup>), although the values are reported by this project as corrosion rate [15].

**Table 7.** Chemical composition of duplex alloys with Gd addition [21-22].

Ref	Fe	Cr	Ni	Mo	N	C	Si	Mn	Gd
21	Bal.	21.929	5.240	3.295	0.048	0.011	0.416	0.600	1.020
22	Bal.	22.25	5.33	2.90			0.45	0.85	0.087

The paper by Jung, et al describes the fabrication and testing of a 0.8% B + 0.5% Gd alloy by ingot casting and hot rolling to a thickness of 3.6 mm [23]. The Korean program seems to have moved away from ferritic based alloys to austenitic based alloys. The researchers used a 316L SS material as a base to add B and Gd during the casting process. The alloy contains 88% austenite and 12% ferrite. The paper does not contain a table of as-cast alloy chemistry. The corrosion test solution chemistry is only defined as a “simulated nuclear waste solution” and the test temperature was not reported.

Table 8 is a shortened version from reference [24] showing PREN values for rolled duplex material. The elemental chemistry values are those for the test material. The PREN values were calculated from this formula (composition in wt.%) which is used for stainless steel materials which have a nitrogen addition to improve pitting resistance:

$$\text{PREN} = [\text{Cr}] + 3.3 [\text{Mo}] + 16 [\text{N}] \quad (\text{Eq. 1})$$

Note that this formula does not account for the possible beneficial effect of W. It should be noted that the PREN values for the alloys discussed in Table 7 are 34 and 33 respectively.

**Table 8.** Duplex and austenitic SS compositions and PREN values.

Type	Specification	Ni	Cr	Mo	N	W	PREN
Austenitic	UNS S31600	10.72	16.75	2.05	-	-	23.5
Super Austenitic	UNS S31254	17.98	20.19	6.26	0.22	-	44.4
Duplex	UNS S31803	5.78	22.53	3.12	0.16	-	35.4
Duplex	UNS S31260	7.13	25.19	3.14	0.16	0.18	38.1
Super Duplex	UNS S39274	6.67	25.10	3.17	0.29	2.13	40.2
Super Duplex	UNS S32750	6.86	25.5	3.82	0.24	-	42.0

**Idaho National Laboratory****Neutron Absorber Material Corrosion Testing Report**

Identifier:

Revision: 0

Effective Date: 09/17/2021

Page 42 of 51

The duplex, super duplex, and super austenitic stainless steels have been developed as intermediate material grades (cost and performance) between a standard marine grade stainless steel for low temperature applications (316L) and the high cost/high performance Ti and Ni-Cr-Mo materials. The PREN values fall far short for those for the Ni-Cr-Mo alloys shown in Table 10.

**Conclusions**

- The duplex stainless steel with Gd and B development and corrosion testing program used an alloy chemistry which would most likely not be suitable in seawater above 30°C.
- The super duplex materials are generally recommended for seawater service up to 50°C.
- The use of a 316L base metal chemistry (powder metallurgy process) with B and Gd additions was marketed in the past by CarTech which is no longer available.
- Based on lack of availability and no indication of adequate corrosion performance, this route is not recommended.

**3.5.2 ANA base material compositions**

The goal of this section is to assess possible improvements to the ANA chemistry (Ni-Cr-Mo-Gd) per ASTM B932) to improve localized corrosion performance [25]. ANA alloy is a nickel-based alloy, where nickel forms an ideal base for accommodating large amounts of alloying elements, interstitial and substitutional, in solid solution. Nickel alloys are produced by dissolving alloying elements into a face centered cubic crystal Ni austenite matrix. The most common alloying elements for a corrosion resistant formulation are Cr and Mo. In contrast to Fe alloys, Ni also can dissolve larger contents of beneficial alloying elements such as Mo without precipitating secondary phases [26].

The original Ni-Cr-Mo alloy (Hastelloy C) was first available in the 1930's for use in seawater and chemical processing service. The nominal chemical composition of this alloy is (in wt.%): Cr-16, Mo-16, W-4, Ni-balance [27]. The alloy has been tested since 1942 at Kure Beach, N.C. (maritime conditions) and exhibited unsurpassed resistance to a seawater atmosphere [27]. Due to the ingot melting practice at the time, this alloy suffered intergranular corrosion in the weld heat affected zone from a high carbon level.

There have been significant improvements in primary melting and secondary refining for Ni-Cr-Mo alloys which resulted in a very low maximum level of carbon. This has resulted in continuous improvement in corrosion performance, mechanical properties, and weldability in the Alloy C family (C, C-276, C4, C-22, C22HS, C-2000) [28]. The allowable chemistry for these and other Ni-Cr-Mo alloys ((Alloy 686 (Special Metals Corporation) and Alloy 59 (VDM Metals International GmbH)) and the ANA composition and corrosion tested alloys are shown in Table 9.

## Idaho National Laboratory

Neutron Absorber Material Corrosion  
Testing Report

Identifier:

Revision: 0

Effective Date: 09/17/2021

Page 43 of 51

**Table 9.** Nickel-based alloy compositions considered in this assessment.

	C4, B575	ANA, B932 (Withdrawn 2010)	C22, B575	M326 (ANA)	M327 (ANA)	C22HS B983	686, B575 (SMC)	59, B575 (VDM)
Mo	14.0-17.0	13.1 – 16.0	12.5-14.5	14.53	14.53	15.5-17.4	15.0-17.0	15.0-16.5
Cr	14.0-18.0	14.5-17.1	20.0-22.5	14.71	21.01	20.0-21.4	19.0-23.0	22.0-24.0
Fe, max	3.0	1.0	2.0-6.0	0.025	0.032	1.8	2.0	1.5
Co, max	2.0	2.0	2.5	0.009	0.003	0.5	-	0.3
C, max	0.015	0.010	0.015	0.006	0.001	0.010	0.01	0.01
Si, max	0.08	0.08	0.08	0.013	0.018	0.08	0.08	0.1
Mn, max	1.0	0.5	0.5	0.001	0.001	0.5	0.75	0.5
P, max	0.04	0.005	0.02	-	-	0.025	0.04	0.015
S, max	0.03	0.005	0.02	0.001	0.002	0.015	0.02	0.001
Ni	remainder	remainder	remainder	-	-	remainder	bal	bal
O <sub>2</sub>	-	0.005	-	0.0032	0.0042	-	-	-
N, max	-	0.010	-	-	-	-	-	-
Gd	-	1.9-2.1	-	2.0	1.98	-	-	-
W	-	-	2.5-3.5	-	-	0.8	3.0-4.4	-
Cu	-	-	0.5 max	-	-	0.5	-	0.5
Va	-	-	0.35 max	-	-	0.5	-	-
Al	-	-	--	-	-	0.5	-	-
Ti	0.7 max	-	-	-	-	-	-	-
Ta	-	-	-	-	-	0.2	-	-
B, max	-	-	-	-	-	0.008	-	-

The present composition of ANA is based on Hastelloy C4 (Haynes International) with a Gd addition.

Recent corrosion tests (including that included here) at the INL show that the best performing ANA chemistry (Heat M327) has a higher Cr level (21% vs 15-16%). The Mo level was somewhat low for this alloy at 14.53 wt%. Recent papers have advanced the concept of higher Cr and Mo levels with a possible W addition for best localized corrosion performance in acidic environments with high levels of chloride [28-32]. Pitting Resistance Equivalent Number (PREN) is an empirical quantity based on the weight percentages of Cr, Mo, and W and has been used to assess nickel alloy corrosion [31]. A higher PREN suggests greater corrosion resistance. The formula to calculate the PREN of Ni based alloys is:

$$\text{PREN} = [\text{Cr}] + 3.3 [\text{Mo}] + 0.5 [\text{W}] \quad (\text{Eq. 2})$$

The authors also describe a more qualitative form for these commercial off the shelf (COTS) alloys exposed to hot chlorides as a systematic trend from the least to most corrosion resistant: - high Cr- low Mo < low Cr – high Mo < high Cr- high Mo < high Cr – high (Mo + W). They describe many caveats in using this approach for choosing Ni-Cr-Mo alloys for any application. A table of PREN values were reported for COTS alloys which is reproduced as Table 10 [31]. The alloys with the highest PREN numbers are: C-22, C-2000, 59, 686, C22HS and Hybrid-BC1.

## Idaho National Laboratory

<b>Neutron Absorber Material Corrosion Testing Report</b>	Identifier:
	Revision: 0
	Effective Date: 09/17/2021

Page 44 of 51

**Table 10.** PREN values of COTS alloys [from reference 31].

Alloy	UNS	Chemical Composition	PREN
<b>825</b>	N08825	43Ni-21Cr-30Fe-3Mo-2.2Cu-1Ti	31
<b>C-276</b>	N00276	59Ni-16Cr-16Mo-4W-5Fe	71
<b>625</b>	N06625	62Ni-21Cr-9Mo-3.7Nb	51
<b>C-22</b>	NO6022	59Ni-22Cr-13Mo-3W-3Fe	66
<b>C-2000</b>	NO6200	59Ni-23Cr-16Mo-1.6Cu	76
<b>59</b>	N06059	59Ni-23Cr-16Mo-1Fe	76
<b>686</b>	N06686	46Ni-21 Cr-16Mo-4W-5Fe	76

**Conclusions:**

Based on the corrosion test results to date and the PREN discussion, the following recommendations for future alloy incorporation (new test material) into the corrosion test program can be made. To provide context, the Cr and Mo compositions and corresponding PREN values have been calculated in Table 11. Note that PREN values are based on Cr and Mo compositions, the effect of Gd cannot be quantified. The present ANA alloy composition with an increased level of Cr and Mo could be produced. The ANA alloys tested early in the corrosion testing program such as M326 had Cr and Mo levels near the lower end of the allowable range (Table 9). If the desire is to meet ASTM B932 specifications, alloys should aim for 17 wt. % Cr and 16 wt. % Mo which are at the top of the allowable compositions. Another possibility is to expand the ANA allowable chemistry from ASTM B932 to match Alloy C4 (18 wt.% Cr and 17 wt.% Mo). This modification would exceed the PREN of M327. Finally, a new M327 inspired composition could be made with an equivalent Cr level of 21 wt.% and higher Mo level of 17 wt.%. The base material for this composition could be Hastelloy C22 HS with a nominal 2 wt.% Gd addition. This composition exhibits a high PREN number but strays far from ASTM B932 compositions (as M327 does). The results of corrosion testing of these proposed alloy formulations may show improved localized corrosion resistance performance due to the increased level of Cr and Mo.

**Table 11.** Existing and proposed new alloy compositions and calculated PREN values for incorporation into the corrosion test program. Note that the detrimental effect of Gd is not quantified (M326 and M327), the table is only considering the Cr and Mo.

Alloy	Cr	Mo	PREN
<b>C4</b>	18	17	73
<b>M326</b>	14.71	14.53	63
<b>ANA (limits of allowable composition)</b>	17.0	16.0	65
<b>M327</b>	21.01	14.53	65
<b>M327 (enhanced)</b>	21	17	77
<b>C22HS</b>	21	17	77

<b>Neutron Absorber Material Corrosion Testing Report</b>	Identifier: Revision: 0 Effective Date: 09/17/2021	Page 45 of 51
---	--	---------------

## 4. Observations

### 4.1 Wrought ANA specimens

#### Observations

- There is conclusive evidence that for lower Cr (16.75% or lower) ANA alloys that corrosion of the secondary phase continues deeper into the specimen.
- For the higher Cr (M327) ANA, penetration deeper into the specimen is not observed in pickling and the material has similarities to the benchmark Ni alloys after surface gadolinide removal.
- M326 with 14.7% Cr shows evidence of base metal corrosion in 1 M HCl and under accelerated electrochemical tests in simulated seawater.
- ANA specimens with intermediate Cr levels (17-20%) were never made, however there is likely no performance gain to be made by reducing Cr from a corrosion perspective.
- A white deposit forms on ANA specimens in seawater, likely precipitation of insoluble gadolinium sulfate and fluoride salts. ANA specimens showing greater corrosion in PS tests (current and charge) had greater deposit formation from qualitative observations.
- The appearance of various ANA alloys after testing are not greatly different after removing deposits. This suggests that corrosion appears closely tied to the gadolinide phase and perhaps regions surrounding the phase. The damage extends into the specimen through some worm-hole pathway. This is supported by cross-sectional SEM images showing signs of microstructures affected are over 100 micrometers deep into the specimen, much greater than the approximately 5 to 10 micrometer particle size.
- Lowering the applied potential closer to the reported  $E_{\text{corr}}$  values (0 V) reduces corrosion significantly (~70X decrease) for a low Cr ANA specimen.
- Alloy 22 does not appear to have any significant advantage over Alloy C-4 in seawater under the tested conditions, both being suitable.

#### Unknowns

- While corrosion is closely tied to the gadolinide phase, we do not know if the base metal immediately surrounding the gadolinides is compromised such that for low Cr specimens this provides a conduit for corrosion to “hop” between secondary phase particles. Close examination of this mechanism pushes the project into more of a research direction which could benefit alloy design but would slow decision making.
- The level of Gd in M326 solutions appears to plateau in pickling tests and this could be examined by repeating M326 pickling for longer times. It could be possible the hopping could be shut down

<b>Neutron Absorber Material Corrosion Testing Report</b>	Identifier:
	Revision: 0
	Effective Date: 09/17/2021

Page 46 of 51

as deeper penetration is reached. In a cave analogy, eventually an end is reached and that the deeper the penetration reaches, the more tortuous path to dissolution and opportunities for precipitate plugging at neutral pH values such as seawater. Note also that in a moist versus fully flooded condition, precipitates may further act to reduce corrosion.

- While higher Cr is a benefit, this study did not have specimens available between 16.75% Cr and 21.1% Cr to assess if a slightly higher Cr levels are adequate. As an example, Alloy C-4 has 18% Cr and appears almost equivalent to Alloy 22 in seawater under the tested conditions.
- Previous work for corrosion of Ni-Cr-Mo has reported the benefit of Mo content [30-31]. Specifically, while Cr was found to reduce initiation of corrosion, increased Mo beneficially impacted the repassivation of alloys [30]. This might be key, considering that dissolution of surface gadolinides effectively requires the exposed primary phase to grow a passive film. New ANA materials should consider increasing Mo content over those reported.

### Recommendations

- With available information, it appears that the higher Cr M327 alloy is suitable in the accelerated corrosion tests. However, since only one ingot of higher Cr ANA exists, it is suggested that performance is confirmed through producing other material should an ingot material be selected.
- If additional ingots are fabricated, it is suggested that a material with about 18-19 % Cr be produced to examine if this is suitable. It also allows a direct comparison with Alloy C-4 and might help explain the base metal corrosion observed in pickling experiments.
- Perform additional microstructural examination of low Cr pickled ANA specimens to examine depth of impact.
- Testing of high Cr ANA is based on one alloy (M327) which limits confidence in results. It is suggested that additional materials be produced to corroborate performance.

### 4.2 ANA coated specimens

#### Observations

- CPP testing showed much greater current that observed for wrought ANA specimens.
- PS tests showed several orders of magnitude higher current than wrought ANA specimens.
- Polishing of the rough as received surface did not result in reduction in corrosion and thus does not explain the increased current for the coatings over wrought material.
- Microstructure and elemental distribution provided in the SNL report [19] shows that Gd is distributed relatively evenly across the surface which may explain the reduction in performance.

#### Unknowns

**Idaho National Laboratory****Neutron Absorber Material Corrosion Testing Report**

Identifier:

Revision: 0

Effective Date: 09/17/2021

Page 47 of 51

- It is likely that crevice corrosion is partially responsible for the loss of performance, but the degree is uncertain.
- It is not known how the gadolinide phases are distributed in the coating and why that leads to poor performance.

**Recommendations**

- Complete the assessment of corrosion by completing the microstructural assessment to help understand why the material is performing poorly.
- Given the poor performance of the cold sprayed coating, if coatings remain a priority for a design it is suggested that a coating method that uses higher temperatures is selected for the next batch of specimens.

**4.3 Stainless steel PS testing****Observations**

- Stainless steel specimens (both 304L and 316L) show a dramatic performance drop with potential and large portions of specimens dissolving. The amount of material loss is significantly greater than any of the wrought nickel alloys tested.
- There is a potential gap between the  $E_{\text{corr}}$  and the potentials where breakdown was observed. However, the 4-hr  $E_{\text{corr}}$  measurement does not allow full equilibration and generally the potentials were trending slowly positive. The  $E_{\text{corr}}$  measurements showed pitting initiation (negative potential spikes) indicative of pitting initiation and repassivation.

**Recommendations**

- It is unlikely that a commercial Grade A BSS will be suitable to the environmental conditions selected for testing (including those up to 60°C).
- Ideally, a BSS would be 316L based Grade A, which does not exist. Should conditions be somewhat milder, this would be a suggested material.

**5. Testing activities for FY22**

After over a year of active testing, greater details on the performance of NAMs in the selected environment have emerged. Unfortunately, not all materials are available or have been produced yet.

Future activities should involve:

- 1) Testing new materials that become available
- 2) Testing promising candidates at higher temperatures

These will be detailed below.

**5.1 New material testing**



## Idaho National Laboratory

<b>Neutron Absorber Material Corrosion Testing Report</b>	Identifier:
	Revision: 0
	Effective Date: 09/17/2021

Page 48 of 51

- SAM2X5 coating testing. The cold spray technique (thermal spray coating) was used to produce corrosion samples using acquired ANA powder by SNL. Amorphous metal powders such as SAM 2X5 have been proposed for corrosion resistant, criticality control applications [33-34]. Coating may be produced by SNL through a separate program (cold spray technique) or may be subcontracted to a vendor and aim to use conditions successfully employed in previous work [33-34].
- Produce and test new wrought ANA material for testing based on Alloy 22 or related high Cr materials and/or M327 alloys. Also consider increased Mo content which has been found to improve repassivation.
- Examine possibility of producing thermal spray coatings consisting of boron carbide powder co-sprayed with Alloy 22 powder.
- Consider generating coatings using existing C22Gd powder using a higher temperature method which could result in microstructure similar to wrought ANA.

### 5.2. Testing of select specimens under more aggressive environmental conditions

- To date several materials can be ruled out of future consideration (assuming these environments): BSS (all commercial grades), Low Cr ANA and cold spray coated ANA. This leaves high Cr ANA as the only material that has been examined suitable to further assessment.
- Examine the effect of temperature by performing experiments above 30°C and below the threshold for criticality. This threshold will be ascertained prior to developing the test matrix.
- Examine the effects of crevice corrosion by testing using crevice washers.

### 5.3. Follow-on activities to support FY21 testing

- Complete analysis of specimens from testing C22Gd coatings produced by cold spray.
- Collect any remaining results from testing and update this report.

### References

- 1) INL PLN 6266, *Neutron Absorber Material Test Plan for FY21*, INL/EXT-21-61320, 2021.
- 2) V. Jain, S.D. Sevougian, P.D. Mattie, K.G. Mon, and R.J. Mackinnon, *Implementation of Localized Corrosion in the Performance Assessment Model for Yucca Mountain*. United States: N. p., 2006. Web. Conference: 2006 International High-Level Radioactive Waste Management Conference, Las Vegas, Nevada, April 30-May 4, 2006.
- 3) G.S. Frankel, *Pitting Corrosion of Metals: A Review of the Critical Factors*, Journal of the Electrochemical Society **145** (1998) 2186.
- 4) R. B. Rebak, *Factors Affecting the Crevice Corrosion Susceptibility of Alloy 22*, NACE Corrosion 2005, Paper 05610, Houston, TX, 2005.
- 5) ASTM G59 – 97 (Reapproved 2014), *Conducting Potentiodynamic Polarization Resistance Measurements*, ASTM International, West Conshohocken, PA.

## Idaho National Laboratory

Neutron Absorber Material Corrosion  
Testing Report

Identifier:

Revision: 0

Effective Date: 09/17/2021

Page 49 of 51

- 6) Hardin, E. 2019. *Technical Memo on Neutron Absorber Materials*. Milestone M5SF-19SN020403023. Albuquerque, NM: Sandia National Laboratory.
- 7) T.E. Lister, R.E. Mizia, A. Erickson and Tammy Trowbridge, *Electrochemical Corrosion Testing of Neutron Absorber Materials*, INL/EXT-06-11772, 2007.
- 8) ASTM D1141 – 99 (2013) *Standard Practice for the Preparation of Substitute Ocean Water*, ASTM International, West Conshohocken, PA.
- 9) D.S. Dunn, O. Pensado, Y.M. Pan, R.T. Pabalan, L. Yang, X. He and K. T. Chiang, *Passive and Localized Corrosion of Alloy 22 — Modeling and Experiments*, CNWRA 2005-02 U.S. Nuclear Regulatory Commission Contract NRC-02-02-012, 2005.
- 10) R. B. Rebak, *Selection of Corrosion Resistant Materials for Nuclear Waste Repositories*, Materials Science and Technology (2006), UCRL-PRDC-221893 (MOL—200610260049).
- 11) R.E. Mizia, T.E. Lister and P.J. Pinhero, *Microstructure and Corrosion Performance of a Neutron Absorbing Ni-Cr-Mo-Gd Alloy*, NACE Corrosion 2003, Paper 03679.
- 12) ASTM G5 – 14 (2014) *Standard Reference Test Method for Making Potentiodynamic Anodic Polarization Measurements*, ASTM International, West Conshohocken, PA.
- 13) ASTM G102 – 89 (2015) *Standard Practice for Calculation of Corrosion Rates and Related Information from Electrochemical Measurements*, ASTM International, West Conshohocken, PA.
- 14) R.E. Mizia and T.E. Lister, *Accelerated Testing of Neutron-Absorbing Alloys for Nuclear Criticality Control*, Nuclear Technology **176** (2011) 9.
- 15) T.E. Lister, R.E. Mizia, L.A. Diaz, M.G. Jones, H.C. Hutcheson, *Neutron Absorber Material Corrosion Testing Final Report*, INL/EXT-20-60774, Rev. 1, 2021.
- 16) P.C. et al. Stevenson, “The Radiochemistry of the Rare Earths, Scandium, Yttrium, and Actinium,” 1961. [Online]. Available: <https://library.lanl.gov/cgi-bin/getfile?rc000021.pdf>.
- 17) D.A. Moreno, B. Molina, C. Ranninger, F. Montero, and J. Izquierdo, *Microstructural Characterization and Pitting Corrosion Behavior of UNS S30466 Borated Stainless Steel*, Corrosion **60** (2004) 573.
- 18) T.E. Lister, R.E. Mizia, A.W. Erickson and B.S. Matteson, *General and Localized Corrosion of Borated Stainless Steels*, NACE Corrosion 2008, Paper 08590, New Orleans, LA, 2008.
- 19) J. Mahaffey and J. Padilla, *Cold Spray of C22Gd Coatings for Nuclear Waste Storage*, Draft Report-SAND2021-10838 R, Sandia National Laboratory, 2021.
- 20) B. Wallen, *Corrosion of Duplex Stainless Steels in Seawater*, Duplex Stainless Steels 97: 5th World Conference / [organized by: Stainless Steel World]. Fifth World Conference on Duplex Stainless Steels, Maastricht, the Netherlands, 21-23 October 1997.
- 21) Y. Choi, B.M. Moon, D.S. Sohn, *Fabrication of Gd Containing Duplex Stainless Steel Sheet for Neutron Absorbing Structural Materials*, Nuclear Engineering and Technology **45** (2013) 684.
- 22) Y. Choi, Y. Baik, B.M. Moon, D.S. Sohn, *Corrosion Wear Properties of Cold Rolled 0.087% Gd Lead Duplex Stainless Steels for Neutron Absorbing Material*, Nuclear Engineering and Technology **48** (2016) 164-168.
- 23) M.Y. Jung, Y. Baik, Y. Choi and D.S. Sohn, *Corrosion and Mechanical Properties of Hot Rolled 0.5%Gd-0.8% B Stainless Steels in a Simulated Nuclear Waste Treatment Solution*, Nuclear Engineering and Technology **51** (2019) 207.

## Idaho National Laboratory

Neutron Absorber Material Corrosion  
Testing Report

Identifier:

Revision: 0

Effective Date: 09/17/2021

Page 50 of 51

- 24) H. Yakuwa, M. Miyasaka, K. Sugiyama and K. Mitsuhashi, *Evaluation of Crevice Corrosion Resistance of Duplex and Super Duplex Stainless Steels for Seawater Pumps*, Paper 09194, NACE Corrosion 2009, NACE International, Houston, TX.
- 25) ASTM B932-04 (2010 withdrawn), *Standard Specification for Low-Carbon Nickel-Chromium-Molybdenum-Gadolinium Alloy*, ASTM International, West Conshohocken, PA.
- 26) N. Shridhar, J.B.C. Wu, P.E. Manning, *Corrosion Resistant Ni-Cr-Mo Alloys*, Journal of Metals November 1985.
- 27) Report, *High Performance Alloys for Seawater Service*, Haynes International, 2021.
- 28) D.C. Agarwal, J. Kloewer, *Nickel Base Alloys: Corrosion Challenges in the New Millennium*, Paper No. 01325, Corrosion 2001, NACE International, Houston, TX.
- 29) A.C. Lloyd, J.J. Noel, S. McIntyre, D.W. Shoesmith, *Cr, Mo, and W alloying additions in Ni and their effect on passivity*, Electrochimica Acta **49** (2004) 3015.
- 30) H.S. Clapper, N.S. Zadorozne and R.B. Rebak, *Localized Corrosion Characteristics of Nickel Alloys: a Review*, Acta Metallurgica Sinica **30** (2017) 296.
- 31) K.L. Cwalina, C.R. Demarest, A.Y. Gerard and J.R. Scully, *Revisiting the effects of Molybdenum and tungsten alloying on corrosion behavior of nickel-chromium alloys in aqueous corrosion*, Current Opinion in Solid State & Materials Science **23** (2019) 129.
- 32) J.D. Henderson, B. Almusned, M. Momeni, S. Anderson, V. Dehnavi, D. Zagidulin, D.W. Shoesmith, and J.J. Noel, *Investigating the Influence of Cr and Mo Additions to Commercial Ni-Based Alloys Exposed to Neutral and Acidic Chloride Solutions*, Journal of the Electrochemical Society **167** (2020) 131512.
- 33) J.C. Farmer, J.S. Choi, C.K. Saw, R. Rebak, S.D. Day, T. Lian, P. Hailey, J.H. Payer, D.J. Branagan and L.F. Aprigliano, *Corrosion Resistance of Amorphous Fe<sub>49.7</sub>Cr<sub>17.7</sub>Mn<sub>1.9</sub>Mo<sub>7.4</sub>W<sub>1.6</sub>B<sub>15.2</sub>C<sub>3.8</sub>Si<sub>2.4</sub> Coating: A New Criticality Control Material*, Nuclear Technology **161** (2008) 169.
- 34) J. Blink, J. Farmer, J. Choi, and S. Saw, *Applications in the Nuclear Industry for Thermal Spray Amorphous Metal and Ceramic Coatings*, Metallurgical and Materials Transactions A **40** (2009) 1344.